GRADUATE AERONAUTICAL LABORATORIES
CALIFORNIA INSTITUTE OF TECHNOLOGY

A STUDY OF WAKES BEHIND A CIRCULAR CYLINDER AT M = 5.7

by

J.F. McCarthy, Jr. and T. Kubota

10 May 1963

Firestone Flight Sciences Laboratory

Guggenheim Aeronautical Laboratory

Karman Laboratory of Fluid Mechanics and Jet Propulsion

Pasadena

A STUDY OF WAKES BEHIND A CIRCULAR CYLINDER AT M = 5.7

by

J.F. McCarthy, Jr. and T. Kubota

10 May 1963

FOREWORD

This paper was prepared for presentation to the Fluid Mechanics Session of the American Institute of Aeronautics and Astronautics Summer Meeting, 17 through 20 June 1963, at Los Angeles.

The study of wakes behind a circular cylinder at M = 5.7 was carried out under the sponsorship and with the financial support of the U.S. Army Research Office and the Advanced Research Projects Agency, contract number DA-04-495-ORD-3231. This research is a part of Project DEFENDER sponsored by the Advanced Research Projects Agency. The work was also supplemented by the Space and Information Systems Division of North American Aviation, Inc.

Dr. McCarthy is Assistant Chief Engineer, Apollo Project, S&ID, North American Aviation, Inc., Downey, California; and Dr. Kubota is Assistant Professor of Aeronautics, California Institute of Technology, Pasadena, California.

CONTENTS

ABSTRACT

The flow field behind a circular cylinder was investigated experimentally at a nominal Mach number of 5.7, over a range of Reynolds numbers from 4500 to 66,500, based on the cylinder diameter. Pitot pressure, static pressure, and total temperature were measured at various distances behind cylinders of three different diameters in order to determine the flow properties in the wake. To correlate data at different Reynolds numbers and to discriminate turbulent wakes from laminar wakes, a linearized theory for the laminar far wake was developed, which included the effects of axial pressure gradient. The transition from laminar flow to turbulent flow was also determined by computing diffusion coefficients from the velocity profiles. The transition thus determined was correlated with the results obtained from mass-diffusion measurements and hot-wire fluctuation measurements.

NOMENCLATURE

A	Constant determined from initial conditions
B	Constant determined from initial conditions
C	Chapman-Rubesin constant in linear viscosity-temperature relation, $C = \frac{\mu_r}{\mu} \frac{T}{T_r}$
c_p	Specific heat at constant pressure
D_N	Diffusivity number, $\lim_{y \to o} \frac{\left(\frac{y}{d}\right)^2}{\ln \frac{w_{\mathfrak{L}}}{w}}$
$\overline{D_N}$	Transformed diffusivity number, $\lim_{\bar{y} \to o} \frac{\bar{y}^2}{\ln \frac{w_{\mathfrak{L}}}{w}}$
d	Cylinder diameter
G	Total-enthalpy excess, $\frac{H}{H_e} - 1$
g	Total-enthalpy ratio, $\frac{H}{H_e}$
H	Total enthalpy
h	Static enthalpy
k	Thermal conductivity
$L_{2\text{-}d}$	Length of two-dimensional flow
M	Mach number
p	Static pressure
p_{atm}	Atmospheric pressure
p_o	Free-stream stagnation pressure, absolute

p_{o_g} Free-stream stagnation pressure, gage

p_p Pitot pressure

Q Heat transfer to the body

Re_d Free-stream Reynolds number based on cylinder diameter, $\frac{\rho_\infty u_\infty d}{\mu_\infty}$

Re_x Reynolds number based on distance along body and conditions at edge of boundary layer

Re_T Townsend Reynolds number, $\frac{(u_e - u_\ell) y_e}{\epsilon_T}$

T Absolute temperature

T_{aw} Adiabatic wire temperature

T_o Stagnation temperature

u Component of velocity parallel to wake centerline

$\bar{u}$ Transformed u, $\frac{u}{u_e}$

v Component of velocity normal to wake centerline

$\bar{v}$ Transformed v

W Dependent variable

w Velocity defect, $1 - \frac{u}{u_e}$

x Length along wake centerline measured from center of cylinder

$\bar{x}$ Transformed x, $\int_o^x \frac{\rho_e \mu_e u_e}{\rho_\infty \mu_\infty u_\infty} \frac{dx}{d}$, measured from neck

$\bar{x_o}$ Effective origin for x upstream of neck

y Length normal to wake centerline measured from line through center of cylinder

$\bar{y}$ Transformed y, $\frac{u_e}{u_\infty}\sqrt{Re_d}\int_o^y \frac{\rho}{\rho_\infty}\frac{dy}{d}$

γ Specific-heat ratio

ϵ_T Turbulent diffusivity

η Variable in y-direction

θ Momentum thickness, $2\int_o^\infty \frac{\rho u}{\rho_e u_e}\left(1-\frac{u}{u_e}\right)dy$

Θ Angle of cylinder measured from stagnation point

μ Dynamic viscosity coefficient

$\tilde{\mu}$ Viscosity parameter, $\frac{\rho\epsilon_T}{\mu}$ for turbulent, 1 for laminar

ν Kinematic viscosity coefficient, $\frac{\mu}{\rho}$

ξ Variable in x-direction

ρ Density

σ Prandtl number, $\frac{c_p\mu}{k}$

χ Hypersonic viscous interaction parameter, $\frac{M_\infty{}^3\sqrt{C_\infty}}{\sqrt{Re_{x_\infty}}}$

Subscripts:

$\mathfrak{C}$ Centerline

e Conditions at outer edge of wake

inv Inviscid

m Measured

r Reference

tr Transition

o Initial conditions (usually taken at neck)

∞ Free-stream conditions

INTRODUCTION

The nature of wakes is one of the oldest basic problems in the field of classical fluid mechanics. Although the low-speed regime of wakes has been discussed in several treatises,* it was only recently that research was directed toward the phenomenon of high-speed flow. The development of intercontinental ballistic missiles and hypersonic reentry vehicles has kindled interest in high-speed wakes.

One of the more interesting aspects of hypersonic wakes is the extreme length of observable phenomena. For example, it is reported by Jacchia that during the descent of the 1957 Soviet satellite, Beta One, the burning object trailed a luminous tail approximately 100 km long.† A comment of Jacchia's concerning the visual observation of Beta One's descent describes the spectacular character of the object's reentry:

> Tail was 25-30 nautical miles long; from white it degraded into dark red and then into a black smoke trail without seeing the end of it.

Contemporary techniques employed in predicting observable phenomena are inadequate, because the theoretical models devised for this purpose have not received experimental confirmation. While some information about gross quantities (i.e., wake width) has been obtained from downrange measurements and ballistic ranges,‡ it is difficult to obtain detailed state properties that would permit the basic structure of the wake to be determined experimentally. For example, Lees and Hromas** were able to confirm

*References 1 to 6.
†Reference 7.
‡References 8 and 9.
**Reference 10.

their theory for turbulent wakes only by shadowgraph and schlieren measurements taken in ballistic ranges; consequently, no confirmation of state properties has thus far been possible. For the laminar-flow regime, the severity of the situation is even more critical because of the dearth of experimental data.

Perhaps the major obstacle in correlating theory and experiment in hypersonic wakes is the difficulty of obtaining reliable and detailed experimental data. Atmospheric reentry involves a temperature and Mach number regime that cannot be effectively simulated by known devices for extended periods. Therefore, only limited data have been secured, either from short-duration experimental facilities (shock tunnels and ballistic ranges) or from actual flight (an expensive technique where results are not easily duplicated). Unfortunately, these data have been inadequate in proving even the most unsophisticated theories of hot, viscous, hypersonic wakes.

One tool generally overlooked in the study of hypersonic wakes is the conventional wind tunnel. Although the wind tunnel does not simulate the high Mach number and the high temperature attained during reentry, it does make possible the confirmation of theoretical models by providing a means of measuring state properties throughout a hypersonic flow field. One major advantage inherent in wind tunnel testing is the capability of varying the Reynolds number—an extremely important parameter in viscous and wake phenomena—independently of other quantities, enabling the Reynolds number effect to be determined explicitly. A systematic hypersonic wake study program, employing the hypersonic wind tunnel as the experimental tool, has been in progress at GALCIT for some time.

Figure 1, which is a schlieren photograph of a circular cylinder at Mach number 5.7, designates the flow field segregated into various classical regions. The classical regions are illustrated in Figure 2. Each region can be treated analytically. After individual analyses, they can be figuratively assembled like a jigsaw puzzle, matching boundary conditions and, if necessary, using iterative procedures. The present investigation is focused upon the wake region shown in Figure 2.

At GALCIT the problem has been grossly divided into three regimes: (1) neck, (2) near wake, and (3) far wake. This paper is the result of one of several investigations of the near wake, a region in which the static pressure has not yet reached the ambient value. Previous investigations have been concerned only with specialized measurements. For example, Demetriades* has investigated transition by hot-wire anemometry; Mohlenhoff† and Kingsland‡ have studied mixing by means of helium and argon diffusion; Dewey** is studying the base-flow region; and Behrens†† investigating the far wake by utilizing thin, heated cylinders as models, is engaged in determining flow properties in the far wake by means of hot-wire anemometry.

Lees and Hromas have indicated several important differences between the low-speed and high-speed wake structure behind blunt bodies; viz., the existence of a stable shear layer (see Figures 1 and 2); the very

---

*Reference 11.
†Reference 12.
‡Reference 13.
**Reference 14.
††Reference 15.

small initial momentum thickness or drag at the neck compared to the total drag of the body; and the lack of evidence of characteristic shedding frequencies, at least in nonionized air at supersonic and hypersonic speeds.

The theoretical problem of hypersonic wakes was first treated by Feldman*, who devised a simple model of the wake flow. Feldman's basic approach has been extended by Lykoudis.† More recently, Lees and Hromas have attacked the problem of turbulent diffusion in the wake by using integral methods to solve the boundary-layer equations. The two-dimensional laminar hypersonic wake with streamwise pressure gradient has been solved by Kubota,‡ using linearized equations.

The purpose of the present investigation is to obtain reliable experimental data of the two-dimensional wake flow behind a circular cylinder—the simplest model that could be devised. With these data supplemented by other experiments, transition from laminar to turbulent flow in the wake can be defined as a function of Reynolds number. Comparison between theory and experiment for the laminar region is then possible.

Three state properties were selected for measurements: (1) pitot pressure, (2) static pressure, and (3) total temperature.

Pitot-pressure measurements drew initial attention because these were obtained accurately and quickly; they could also be used to define the geometry of the flow field as well as determine one state property.

---

*Reference 16.
†Reference 17.
‡Reference 18.

An experimental verification was attempted to demonstrate that the static pressure was nearly constant with vertical distance in the wake (as expected from theory). Static pressures were also employed to determine the two-dimensionality of the flow field. Finally, axial traverses were made along the centerline to obtain a second state property.

Minimum effort was expended in determining total-temperature because the model used was almost completely insulated; thus, only slight variations in total temperature were present. However, sufficient total-temperature data were gathered to determine the dependence of this state property on free-stream Reynolds number. In the process of investigating the near-wake characteristics, it was necessary to make base-pressure measurements in order to extrapolate static-pressure data upstream.

Once the flow field was established experimentally, the data were used to define transition from laminar to turbulent flow to separate these two regimes.

EXPERIMENTAL TECHNIQUES

GALCIT HYPERSONIC WIND TUNNEL

All tests were conducted in the GALCIT hypersonic wind tunnel, leg 1 (Figure 3). The test section of this tunnel is 5 inches in width and 5 1/4 inches in height. The wind tunnel is a continuous-flow, closed-return device, with a nominal fixed Mach number of 5.7 in the region where the model was ultimately placed (17.34 inches from the throat). A complete description

of the compressor and the associated instrumentation is given by Baloga and Nagamatsu.*

The reservoir pressure ranged from 0.00 to 100.00 psig, with an accuracy of ±0.02 psig and with corresponding Reynolds numbers between 33,000 and 260,000 per inch, based on free-stream conditions. The automatically controlled reservoir temperature can be varied between 225 and 325 F. A reservoir temperature of 262 F was selected for all tests. This temperature closely approached the minimum for good flow without condensation effects for the nominal operating dew points. The maximum temperature was limited to approximately 275 F by the saran tubing used in the pressure-recording systems. The reservoir temperature could be maintained constant to within ±1 F. The nominal operating dew point was less than -40 F; however, after approximately eight hours of steady testing, the dew point began to deteriorate. No data were taken at dew points higher than -25 F.

On the basis of preliminary measurements, the models were located at 17.34 inches from the throat (Figure 3). The downstream limitation of flow uniformity was determined by disturbances originating slightly upstream of the junction of the model with the wind tunnel's sidewalls (discussed later in this section) and not by the test-section rhombus.

*Reference 19.

Table I. Test Summary

Model d (inch)	p_{o_g} (psig)	T_o (^oF)	Re_d ($x10^{-3}$)
0.300	85.00	263	66.5
0.300	60.00	263	49.4
0.300	35.00	262	32.7
0.300	10.00	262	16.7
0.200	96.68	264	49.3
0.200	59.48	263	32.7
0.200	22.48	262	16.6
0.200	3.80	260	8.58
0.100	59.42	263	16.3
0.100	22.54	262	8.28
0.100	3.84	260	4.29

Table I indicates that an attempt was made to duplicate Reynolds number by varying both the density and the model size. An exact duplication was not possible because of the variations in free-stream Mach number caused by stagnation pressure changes that influence boundary-layer thickness on the nozzle walls. The 3-to-1 ratio in model size and the 6-to-1 ratio in absolute stagnation pressure promised the possibility of obtaining a sufficient variation in Reynolds number to determine its effect on wake properties.

PITOT-PRESSURE MEASUREMENTS

Obtaining reliable, experimentally verified, total-pressure surveys at various axial distances in the wake and the adjacent inviscid flow region constituted one of the experimental program's major efforts. This total pressure not only provides one flow parameter but also represents an accurate measurement of wake geometry.

The small variable-reluctance differential pressure transducer shown in Figure 4 was selected as the basis for a very low-time-constant pressure-recording system. The volume of the transducer with its glass measuring tip was very small; also, the length of the tubing from the probe tip to the transducer was minimal, so that the time constant was minimized. The time constant of this pressure-recording system was about 50 milliseconds. This was determined by driving the probe through the bow shock generated by the cylindrical model.

The reference side of the transducer was connected to a vacuum reference, and the measuring side of the transducer was connected to the glass tip (about 1-inch long with the dimensions shown in Figure 5). The outside diameter at the apex of the glass tip was selected at 0.039 inch, small enough to obtain satisfactory resolution and large enough to minimize the effects of Reynolds number.

To calibrate the transducer, another glass tip of exactly the same geometry as the original measuring glass tip was located a known distance, 0.149 inch, below the measuring tip (Figure 5). This calibration tip was connected to a mercury micromanometer with which pressures could be measured to 0.001 cm mercury.

The pressure transducer was used with a CEC carrier amplifier, which furnished a 5-volt 20-kilocycle carrier signal and amplified and demodulated the output from the transducer, producing as final output a dc-signal up to 75 millivolts. Since the output was sensitive to the temperature to which the transducer was subjected and which varied over a large range, the transducer was housed in a head that was water-cooled to provide a constant temperature during a vertical traverse (Figure 4). The temperature of the transducer was monitored by cementing a standard thermocouple on the transducer case (see Figures 4 and 5).

The pitot-pressure probe was moved vertically from outside the tunnel by lead-screws activated by a motor. The probe-positioning gearing turned the helipot potentiometer that converted the probe position to a linear electrical signal that was fed into the autograph recorder. The system block diagram is shown in Figure 6.

The calibration procedure was to record the final voltage output of the pressure-recording system, move the probe vertically 0.149-inch, and measure the pressure with the mercury micromanometer. All calibrations were obtained with the pressure-recording system installed ready for use. Pressure was varied by changing the stagnation pressure of the wind tunnel.

Axial positioning was provided by another driving mechanism. The axial position of the probe was determined by a counter attached to the axial driver. The counter was calibrated after temperature equilibrium was established through several hours of wind tunnel operation.

Finally, because flow inclinations up to 15 degrees were encountered in the flow field, measurements were made to determine the angle-of-attack sensitivity of the pitot probe. The results of this calibration showed that the pitot probe is relatively insensitive to angle of attack in the range of interest (±15 degrees). Estimated accuracy of the pitot-pressure measurements is $\Delta p_p/p_o = \pm 10^{-4}$.

Typical pitot-pressure traces are shown in Figure 7. Isoaxiometric visualization of the entire flow fields for two typical cases are shown in Figures 8, 9, and 10. Figure 9 shows the flow field around the neck region illustrated in Figure 8. Figure 8 represents a turbulent case, and Figure 10 represents a laminar case.

STATIC-PRESSURE MEASUREMENTS

The static pressure was measured by means of a small probe connected to a sensitive variable reluctance transducer located outside the wind tunnel (Figure 11). The entire system was outgassed for several weeks before recording final data. The reference pressure on the transducer was maintained at approximately four microns of mercury; it was measured by a Stokes gauge equipped with a liquid-nitrogen cold trap. As with the pitot-pressure measurements, the static-pressure recording system was calibrated by varying the stagnation pressure of the wind tunnel over a wide range. The CEC carrier amplifier was used also for the static-pressure recording system (Figure 6).

To establish the fact that the pressure was nearly constant across the viscous wake, as expected from theory, several vertical static-pressure

surveys were made for various-sized cylinders at different axial locations. A typical vertical static-pressure survey is shown in Figure 12. It should be noted that the static pressure is constant across the wake and almost constant up to the trailing shock.

To test the two-dimensionality of the flow field behind the cylindrical rod, the static-pressure distribution was measured in the horizontal direction parallel to the cylinder axis. Several trace surveys were made at various axial positions downstream of the 0.300-inch and 0.100-inch models. These surveys revealed that a disturbance originated ahead of the intersection of the model with the sidewalls of the wind tunnel. As a result of these tests, the limits of two-dimensional flow (Figure 13) were identified. As noted in Figure 13, the distance, L_{2-d}, was a function of model size and wind tunnel stagnation pressure.

As with the pitot-pressure probe, the angle-of-attack sensitivity of the static-pressure probe was determined. Unlike the pitot-pressure measurements, however, the flow inclination around the static-pressure probe is very nearly zero; therefore, the only error in angle of attack is due to installation, which is estimated to be accurate to less than one degree (the order of magnitude of the flow uniformity).

After establishing that the pressure was nearly constant across the wake and after identifying the boundaries of the two-dimensional region behind the model, static-pressure traces were taken along the centerline of the wind tunnel and behind the models for the eleven conditions cited in Table I.

The results of these tests are shown in Figure 14. The static-pressure traces were again checked by measuring the pressure at several different stations on various days. Estimated accuracy of the static-pressure measurements is $\Delta p/p_\infty = \pm 0.005$. All axial static-pressure traces were supplemented by corresponding tunnel-empty surveys.

The orifices of the static-pressure probe were located a fixed distance behind the apex of the probe cone; therefore, it was not possible to obtain experimental values of static pressure close to the neck. Consequently, it was necessary to estimate the static pressure in the vicinity of the neck from available data. Unfortunately, because the axial gradient in static pressure is high, the extrapolation upstream of the measured data is inaccurate unless a value of the static pressure at the neck is available. The static pressure slightly behind the neck was estimated by considering the base flow region.*

TOTAL-TEMPERATURE MEASUREMENTS

Total temperature was measured by an unshielded thermocouple with heated supports, shown in Figure 15. The heating of supports was controlled, so that the support temperature was equal to the temperature indicated by the thermocouple.

Because each total temperature trace required several hours, only the traces shown in Figure 16 were taken with the corresponding tunnel-empty data. These traces were considered adequate for defining total-temperature variation in the wake as a function of Reynolds number, especially since the

*Reference 20.

percentage variation of absolute temperature was small, (except in the vicinity of the neck) even for laminar flow.

When the tunnel-empty data were reduced, they confirmed the calibration of reservoir temperature to within 3 F. This difference is well within the value of $T_{aw}/T_o = 0.95 \pm 0.01$ for continuum flow given by Laufer and McClellan.* Although the absolute level of free-stream total temperature was accurate to within 3 F, the accuracy of total-temperature distributions is even more satisfactory because they represent variations from a reference value. The accuracy of the thermocouple measurements is estimated at $\pm 1/2\,^{\circ}F$.

BASE-PRESSURE MEASUREMENTS

To extrapolate the measured static-pressure traces in the wake upstream, it was necessary to measure the base pressure of the model accurately. Only the 0.300-inch diameter cylinder was used because of the finite size of the static-pressure orifices. The 0.009-inch diameter orifice (Figure 17) was as small as practicality permitted, and it corresponded to about 3 degrees for the 0.300-inch diameter.

This experiment utilized three holes to check data duplicability; this was accomplished by blocking one or two holes. After duplicability was established, the time constant of the total system was considerably reduced by simultaneous use of the three holes. The pressure-recording system for this experiment was identical to the system discussed earlier for static-

*Reference 21.

pressure measurements. The calibration counter (Figure 17) had a 100-to-1 turn ratio, permitting the angles to be measured to ±0.01 degree.

The base-pressure measurements determined by this experiment are shown in Figure 18b. This figure also plots the authors' best estimate of the data of Tewfik and Giedt,* whose experiments were made at a much lower Reynolds number than the present tests. In Figure 18b, the region of reverse flow is evident, especially at high stagnation pressure. Accuracy of the base-pressure measurements was estimated at $\Delta p(\theta)/p(0) = \pm 0.02$ for the lowest stagnation pressures, as determined by the symmetry of the experimental data about the rear stagnation point. For the highest stagnation pressures, the accuracy was estimated at $\Delta p(\theta)/p(0) = \pm 0.01$.

Demetriades† integrated the pressures obtained from this experiment and calculated a drag coefficient of 1.27 for the cylindrical rod, compared to the value of 1.2 to 1.3 predicted by Ferri.‡ The pressure distributions obtained are shown in Figure 18a. This figure also plots the values of Tewfik and Giedt. The accuracy of the data of Figure 18a was limited only by the graphical reading error and the finite size of the pressure orifices $(p(\theta)/p(0) = \pm 0.002)$.

As seen in Figure 18a, the dimensionless pressure distribution around the cylinder up to $\theta = 90$ degrees is practically independent of Reynolds number in the range considered. This is attributable to the fact that the

*Reference 22.
†Reference 23.
‡Reference 24.

effective shape of the cylinder does not change appreciably. It is obvious that the base pressure is a function of Reynolds number.

DATA REDUCTION

Reynolds number corrections to measured pitot pressures may be necessary for very low Reynolds numbers, but for the present tests, the outside diameter of the glass tip used for pitot measurements (Figure 5) was chosen to preclude corrections when reducing the experimental data. No account was taken of the effective displacement of streamlines caused by velocity gradients present in the wake. This correction was estimated to be less than 10 percent of the wake width for the worst case, i. e., in the vicinity of the neck.

To correct the values of static pressure for boundary-layer effects, as measured by the probe shown in Figure 11, Matthews' data, which were taken for static-pressure probes of the same geometry as that used for the present tests, were used. * Based on his data, a value of the viscous interaction parameter, χ, was calculated. A linear variation was then assumed for the value of measured pressure to ideal pressure, as a function of the viscous interaction parameter

$$\frac{p_m}{p} = 1 + 0.235\,\chi \qquad (1)$$

This variation is less than that for an insulated flat plate as discussed by Hayes and Probstein.†

*Reference 25,
†Reference 26, p. 349.

The temperature measured by the heated thermocouple is the adiabatic wire temperature associated with infinite aspect ratio. However, the adiabatic wire temperature must be corrected for the recovery factor to obtain the true total temperature. This correction was accomplished with data based on Dewey's work. For free-molecule flow and continuum flow, the ratios of adiabatic wire temperature to total temperature are 7/6 and 0.95, respectively.

As noted in the preceding portions of this section, the accuracy of each measurement was carefully identified. However, because of the many involved calculations necessary in obtaining final data, the accuracy of the final product can only be roughly estimated. It is estimated that the over-all accuracy of the final experimental data is from 2 to 4 percent for the distributions of normalized velocity, static enthalpy, and total enthalpy, except in the immediate region of the neck. It is estimated that the computed absolute values of the centerline quantities is accurate to within 5 percent. The major source of error was the extrapolation of static pressure into the neck region.

RESULTS AND DISCUSSION

Before discussing the experimental results, a linearized laminar-wake theory is discussed briefly. It is assumed that the flow in the viscous wake is described by the boundary-layer equations. By introducing the following transformation

$$\bar{x}(x) = \int_0^x \frac{\rho_e \mu_e u_e}{\rho_\infty \mu_\infty u_\infty} \frac{dx}{d} \qquad (2)$$

$$\bar{y}\,(x,\ y) = \frac{u_e}{u_\infty}\sqrt{Re_d}\ \int_o^y \frac{\rho}{\rho_\infty}\,\frac{dy}{d}\,, \tag{3}$$

the differential equations become

$$\bar{u}\,\frac{\partial \bar{u}}{\partial \bar{x}} + \bar{v}\,\frac{\partial \bar{u}}{\partial \bar{y}} = (g - \bar{u}^2)\,\frac{1}{M_e}\,\frac{dM_e}{d\bar{x}} + \frac{\partial^2 \bar{u}}{\partial\, \bar{y}^2} \tag{4}$$

$$\bar{u}\,\frac{\partial g}{\partial \bar{x}} + \bar{v}\,\frac{\partial g}{\partial \bar{y}} = \frac{1}{\sigma}\,\frac{\partial^2 g}{\partial \bar{y}^2} - \frac{1-\sigma}{\sigma}\,\frac{(\gamma-1)\,M_e^2}{1+\frac{\gamma-1}{2}M_e^2}\,\frac{\partial}{\partial \bar{y}}\left(\mu\,\frac{\partial \bar{u}}{\partial \bar{y}}\right) \tag{5}$$

where,

$$\bar{u} = \frac{u}{u_e} \tag{6}$$

and,

$$g = \frac{H}{H_e} = \frac{(1/2)\,u^2 + h}{(1/2)\,u_e^2 + h_e}\,. \tag{7}$$

The boundary conditions become

$$\bar{u}\,(x,\ \pm\infty) = g\,(x,\ \pm\infty) = 1 \tag{8}$$

$$\frac{\partial \bar{u}}{\partial \bar{y}}\,(x,\ 0) = \frac{\partial g}{\partial \bar{y}}\,(x,\ 0) = 0\,. \tag{9}$$

It is assumed that the Prandtl number is constant (not necessarily = 1), and, analogous to the Chapman-Rubesin relation for linear temperature-viscosity relationship,

$$\rho\mu = \rho_e\,\mu_e\,. \tag{10}$$

In order to linearize Equations 4 and 5, let

$$\bar{u} = 1 - w \tag{11}$$

$$G = g - 1 \tag{12}$$

and assume the velocity defect, $w << 1$. Substituting into Equations 4 and 5

and retaining lowest-order terms, we obtain

$$\frac{\partial}{\partial \bar{x}} \left(\frac{h}{h_e} - 1 \right) = \frac{1}{\sigma} \frac{\partial^2}{\partial \bar{y}^2} \left(\frac{h}{h_e} - 1 \right) \tag{13}$$

$$\frac{\partial}{\partial \bar{x}} \left(M_e^{\,2} w \right) + G \frac{dM_e}{d\bar{x}} = \frac{\partial^2}{\partial \bar{y}^2} \left(M_e^{\,2} w \right) \tag{14}$$

where

$$\frac{h}{h_e} - 1 = (\gamma - 1) M_e^{\,2} w + \left(1 + \frac{\gamma - 1}{2} M_e^{\,2} \right) G \tag{15}$$

with the boundary conditions

$$\left.\begin{aligned} G &= o \\ w &= o \end{aligned}\right\} \text{ at } \begin{aligned} \bar{x} &= \infty \\ \bar{y} &= \pm\infty \end{aligned} \tag{16}$$

$$\left.\begin{aligned} \frac{\partial w}{\partial \bar{y}} &= o \\ \frac{\partial G}{\partial \bar{y}} &= o \end{aligned}\right\} \text{ at } \bar{y} = o \tag{17}$$

If

$$G << w, \tag{18}$$

Equations 13 and 14 reduce to the diffusion equation

$$\frac{\partial W}{\partial \xi} = \frac{\partial^2 W}{\partial \eta^2} \tag{19}$$

Thus, the solutions of Equations 13 and 14 for $G << w$ and initial delta functions at the origin of $\bar{x}$ are

$$M_e^{\,2} w = \frac{A}{\sqrt{\bar{x}}} \exp\left(- \frac{\bar{y}^2}{4\bar{x}} \right) \tag{20}$$

$$\frac{h}{h_e} - 1 = \frac{B}{\sqrt{\bar{x}}} \exp\left(- \frac{\sigma \bar{y}^2}{4\bar{x}} \right) \tag{21}$$

where A and B are determined from the initial condition (usually taken at the neck)

$$A = 1/2 \sqrt{\frac{Re_d}{\pi}} \left(\frac{\rho_e u_e \theta}{\rho_\infty u_\infty d} M_e^2 \right)_o \tag{22}$$

$$B = \frac{\sqrt{\sigma Re_d}}{2\sqrt{\pi}(\rho_\infty u_\infty d) h_{e_o}} \left[Q + (\rho_e u_e^3 \theta)_o \right] \tag{23}$$

θ is the momentum thickness

$$\theta = 2 \int_o^\infty \frac{\rho u}{\rho_e u_e} \left(1 - \frac{u}{u_e} \right) dy \tag{24}$$

and Q is the heat transfer to the body.

From Equation 22

$$\frac{\theta}{\theta_o} = \frac{(\rho_e u_e M_e^2)_o}{\rho_e u_e M^2} \tag{25}$$

As shown in the given equations, the value of the momentum thickness and wake width at the neck must be known as initial conditions for theoretical analyses. Lees and Hromas have estimated these quantities and shown that they should vary as $(Re_d)^{-1/2}$ based on estimates of skin friction around the body and the pressure rise at the neck. Experimental values, based on the present tests, are shown in Figure 19. In Figure 19, eleven points are shown corresponding to the combinations of cylinder diameter and Reynolds number given in Table I. The wake width was obtained from pitot-pressure measurements, and the momentum thickness was calculated from experimental data. The axial location of the neck was taken at x/d = 2.50 for the 0.300-inch diameter cylinder and x/d = 3.00 for the other models. Figure 19

shows that these quantities do vary as $(Re_d)^{-1/2}$ The scatter of Figure 19 is probably due to the effect of the velocity gradient on pitot measurements. The exact axial location of the neck, which varies with Reynolds number, was not known.

The analysis shows the $\left(\frac{h}{h_e} - 1\right)$ and $M_e^2 w$ vary as $(\bar{x})^{-1/2}$ along the wake centerline. The results from the experiments are plotted in Figures 20 and 21. Figures 20 and 21 show that there is definitely a Reynolds number correspondence for the laminar theory. The two runs which do not correspond with the base line are interpreted to be fully turbulent. It should be noted that the static-enthalpy excess and the velocity defect for the turbulent case also varies as $(\bar{x})^{-1/2}$, when turbulence is fully established. The representations of Figures 20 and 21 can also be used as measures of transition. At transition, the values of velocity defect and static-enthalpy excess decrease much more rapidly than for the laminar case because of more efficient mixing processes.

Since the velocity and the temperature in the inviscid flow outside of the viscous wake are not constant but vary parabolically, the viscous contribution to the profile was obtained by subtracting the extrapolation of the inviscid profile into the viscous region. This is perfectly consistent with the spirit of the laminar boundary-layer theory. When the velocity and the temperature from the experiment are plotted against the square of the distance from the wake centerline, the points lying outside the viscous wake fall on a straight line, which can be easily extended into the viscous region (Figure 22). The viscous profiles thus obtained are plotted in Figures 23 and 24 for

the lowest Reynolds number cases for the 0.100-inch and the 0.200-inch diameter cylinders (Table 1). The form of the abscissa is suggested by the foregoing analysis and avoids the ambiguity of defining the wake edge. The additive constant, $\bar{x}_o$, in Figure 24, is the location of the virtual origin of the wake, determined from the variation of the centerline velocity and temperature.* For the 0.100-inch diameter cylinder, there is good agreement between the experiment and the linearized theory beyond nine diameters downstream. Evidently, for the region of the wake closer to the neck, the constant convection assumption used for linearization ($w \ll 1$) is no longer valid.

Lees and Hromas assumed the Townsend value of "universal" turbulent Reynolds number of 12.5 for the centerline conditions in the turbulent wake. To investigate this assumption experimentally, consider the momentum equation at the centerline.

$$\rho_{\text{℄}}\, u_{\text{℄}} \left(\frac{\partial u}{\partial x}\right)_{\text{℄}} + \frac{dp}{dx} = \rho_{\text{℄}}\, (\epsilon_T)_{\text{℄}} \left(\frac{\partial^2 u}{\partial y^2}\right)_{\text{℄}} \tag{26}$$

In order to obtain $\frac{\partial^2 u}{\partial y^2}$ without differentiating experimental data twice, the method first proposed by Kingsland to reduce diffusion measurements was used. Assuming that the velocity profile near the center is close to Gaussian,

$$\frac{w}{w_{\text{℄}}} = 1 - a \left(\frac{y}{d}\right)^2 + \ldots . \tag{27}$$

*Reference 20.

we obtain

$$\frac{\ln \frac{w}{w_{\mathfrak{C}}}}{\left(\frac{y}{d}\right)^2} = -a \tag{28}$$

giving

$$\left(\frac{\partial^2 u}{\partial\left(\frac{y}{d}\right)^2}\right)_{\mathfrak{C}} = u_e \frac{2w_{\mathfrak{C}}}{D_N} \tag{29}$$

where the diffusivity number is defined by

$$D_N = \lim_{y \to o} \frac{\left(\frac{y}{d}\right)^2}{\ln \frac{w_{\mathfrak{C}}}{w}} = \left[\frac{d\left(\frac{y^2}{d^2}\right)}{d\left(\ln \frac{w_{\mathfrak{C}}}{w}\right)}\right]_{y=o} \tag{30}$$

Plots of the parameter, $\sqrt{\ln \frac{w_{\mathfrak{C}}}{w}}$, versus vertical distance near the centerline are shown in Figure 25 for a typical case (Table I). From these plots it was then possible to obtain the diffusivity number.

Once D_N is determined, $(\epsilon_T)_{\mathfrak{C}}$ is given by

$$\left(\frac{\epsilon_T}{\nu}\right)_{\mathfrak{C}} = \frac{D_N d^2 \left(\rho u \frac{\partial u}{\partial x} + \frac{dp}{dx}\right)_{\mathfrak{C}}}{2\mu_{\mathfrak{C}} (u_e - u_{\mathfrak{C}})} \tag{31}$$

The expression on the right-hand side of the above relation is equal to unity in laminar wakes and greater than unity in turbulent wakes. Figure 26 presents this expression, denoted by $\tilde{\mu}$, evaluated for several cases. It shows that $\tilde{\mu}$ is about unity in low Reynolds number cases, grows greater than unity at downstream stations in medium Reynolds number cases, and is larger than unity throughout the wake in the highest Reynolds number case.

The Townsend Reynolds number Re_T is defined by

$$Re_T = \frac{(u_e - u_{\mathfrak{L}})y_e}{\epsilon_T} \tag{32}$$

This definition of Re_T differs slightly from that of Reference 4, where, in place of y_e, the length used is the distance from the center at which the velocity defect is $e^{-1/2}$ of the maximum defect.

To obtain experimental values of the Townsend Reynolds number, it is necessary to differentiate two experimental quantities that subtract from each other to evaluate the turbulent diffusivity (Equation 31). Therefore, the accurate determination of this quantity is very difficult. In any case, the tentative value, $Re_T = 10 \pm 5$, was obtained. This value agrees very well with that used by Lees and Hromas in their theoretical treatment ($Re_T = 12.5$). The results also compare favorably with those of Kingsland, where he estimated the value, $Re_T = 12$.

EXPERIMENTAL DETERMINATION OF TRANSITION

As indicated in the foregoing discussion, a qualitative definition of transition could be obtained from plots of state properties along the centerline. Another definition is possible by calculating the Townsend Reynolds number discussed previously. Perhaps the best definition, however, was obtained from plots of transformed diffusivity number, $\bar{D}_N$, versus axial distance.*

*Reference 20

Using all available inputs, the results for these tests are superimposed on those of Demetriades[†] in Figure 27. For the eleven runs shown in Table I, seven transition points could be obtained—two cases being fully laminar and two cases fully turbulent. The comparison with Demetriades' data is surprisingly good. Since the edge properties could be determined with the present measurements, it was possible to define a transition Reynolds number based on local conditions and distance from an effective origin. Its value was calculated as 85,000.[‡]

CONCLUSIONS

An experimental investigation has been made of the flow behind a circular cylinder at a nominal free-stream Mach number of 5.7. The Reynolds number was varied by changing both the diameter of the cylinder and the stagnation pressure of the wind tunnel—the former over a three-fold range and the latter over a six-fold range. Enough measurements were made to completely define the flow field at various stations downstream.

From these measurements, it is concluded that (1) the base flow region is laminar for the entire range of Reynolds number in the present experiment, (2) static pressure is nearly constant across the wake, (3) the near wake is laminar for low Reynolds number cases and becomes turbulent as Reynolds

[†]Reference 11

[‡]Further discussion of transition incorporating these data is given in Reference 27.

number is increased, and (4) the transition in the wake occurs when the Reynolds number based on edge conditions and the distance from the body exceeds 85,000.

A linearized laminar wake theory was developed based on the Oseen approximation. Correlation of the experimental data with theory for laminar flow was then made. The theoretical prediction of centerline values of static enthalpy and local velocity based on this theory were in excellent agreement with the experimental results. Distributions of static enthalpy and local velocity in the wake agree with the theory for downstream stations greater than about nine diameters, if provision is made for an "effective" origin based on the axial distribution of the velocity and the enthalpy at the centerline.

A qualitative experimental value of the Townsend Reynolds number for turbulent flow on which the theory of Lees and Hromas is based was obtained. Its value was determined as $Re_T = 10 \pm 5$. In the present experiments, accurate definition of the turbulent wake was very difficult since the pitot pressure defect decays very rapidly in the turbulent wake. Further experiments are needed to investigate the turbulent wakes in hypersonic flow, especially the effect of interaction with external vorticity.

REFERENCES

1. Goldstein, S. (editor). Modern Developments in Fluid Dynamics, Vol. II, Chapter XIII. London: Oxford University Press, 1938.

2. Schlichting, H. Boundary Layer Theory, 4th ed. New York: McGraw-Hill Book Company, Inc., 1960.

3. Birkhoff, G. and E.H. Zarantonello. Jets, Wakes, and Cavities. New York: Academic Press, Inc., 1957.

4. Townsend, A.A. The Structure of Turbulent Shear Flow. London: Cambridge University Press, 1956.

5. Roshko, A. On the Drag and Shedding Frequency of Bluff Cylinders. NACA TN 3169 (July 1954).

6. Cooper, R.D. and M. Lutzky. Exploratory Investigation of the Turbulent Wakes Behind Bluff Bodies. The David W. Taylor Model Basin, Research and Development Report 963 (October 1955).

7. Jacchia, L.G. The Descent of Satellite 1957 Beta One. Smithsonian Institution Astrophysical Observatory Special Report No. 15, Optical Satellite Tracking Program (20 July 1958).

8. Slattery, R.E. and W.G. Clay. Width of the Turbulent Trail Behind a Hypervelocity Sphere. M.I.T. Lincoln Laboratory. Report 35 G-0004 (6 June 1961).

9. Dana, T.A. and W.W. Short. Experimental Study of Hypersonic Turbulent Wakes. Convair, San Diego. Report ZPh-103 (29 May 1961).

10. Lees, L. and L. Hromas. Turbulent Diffusion in the Wake of a Blunt-Nosed Body at Hypersonic Speeds. Space Technology Laboratories, Inc., Aerodynamics Department Report 50 (July 1961). Also, Institute of Aerospace Sciences paper No. 62-71, presented at the IAS 30th annual meeting, New York, New York, 22-24 January 1962.

11. Demetriades, A. Some Hot-Wire Anemometer Measurements in a Hypersonic Wake. Proceedings of the 1961 Heat Transfer and Fluid Mechanics Institute. Stanford University Press, 1961.

12. Mohlenhoff, W. Experimental Study of Helium Diffusion in the Wake of a Circular Cylinder at M = 5.8. GALCIT Hypersonic Research Project Memorandum No. 54 (20 May 1960).

13. Kingsland, L., Jr. Experimental Study of Helium and Argon Diffusion in the Wake of a Circular Cylinder at M = 5.8. GALCIT Hypersonic Research Project. Memorandum No. 60 (1 June 1961).

14. Dewey, C.F., Jr. Hot-Wire Measurements in Low Reynolds Number Hypersonic Flows. GALCIT Hypersonic Research Project. Memorandum No. 63 (15 September 1961). Also, American Rocket Society Journal, (December 1961),1709-1718.

15. Semi-Annual Status Report. GALCIT Hypersonic Research Project (April 1962).

16. Feldman, S. On Trails of Axi-Symmetric Hypersonic Blunt Bodies Flying Through the Atmosphere. AVCO-Everett Research Laboratory. Research Report No. 82 (December 1959). Also, Journal of the Aerospace Sciences, Vol. 28, No. 6 (June 1961), 433-448, 470.

17. Lykoudis, P.S. Theory of Ionized Trails for Bodies at Hypersonic Speeds. The RAND Corp. Report No. RM-2682-1-PR (29 May 1961, revised 5 October 1961).

18. Kubota, T. Laminar Wake With Streamwise Pressure Gradient. GALCIT Hypersonic Research Project. Internal Memorandum No. 9 (1 May 1962).

19. Baloga, P.E. and H.T. Nagamatsu. Instrumentation of GALCIT Hypersonic Wind Tunnels. GALCIT Memorandum No. 29 (31 July 1955).

20. McCarthy, J.F., Jr. Hypersonic Wakes. Ph.D. Thesis, Aeronautics Department, California Institute of Technology (1962). Also GALCIT Hypersonic Research Project. Memorandum No. 67 (2 July 1962).

21. Laufer, J. and R. McClellan. "Measurements of Heat Transfer from Fine Wires in Supersonic Flows." Journal of Fluid Mechanics, Vol. 1, No. 3 (September 1956), 276-289.

22. Tewfik, O.K. and W.H. Giedt. Heat Transfer, Recovery Factor and Pressure Distributions Around a Cylinder Normal to a Supersonic Rarefied Air Stream, Part I, Experimental Data. University of California, Berkeley. Technical Report HE-150-162 (30 January 1959). Also, Journal of the Aerospace Sciences, Vol. 27, No. 10 (October 1960), 721-729.

23. Demetriades, A. Private Communications, 1961-2.

24. Howarth, L. (editor). Modern Developments in Fluid Dynamics, High Speed Flow. Vol. II. Oxford: Clarendon Press, 1953. 684.

25. Matthews, M.L. An Experimental Investigation of Viscous Effects on Static and Impact Pressure Probes in Hypersonic Flow. GALCIT Hypersonic Research Project. Memorandum No. 44 (2 June 1958).

26. Hayes, W.D. and R.F. Probstein. Hypersonic Flow Theory. New York: Academic Press, 1959.

27. Demetriades, A. and H. Gold. "Transition to Turbulence in the Hypersonic Wake of Blunt-Bluff Bodies." ARS Journal, Vol. 32, No. 9 (September 1962), 1420-1421.

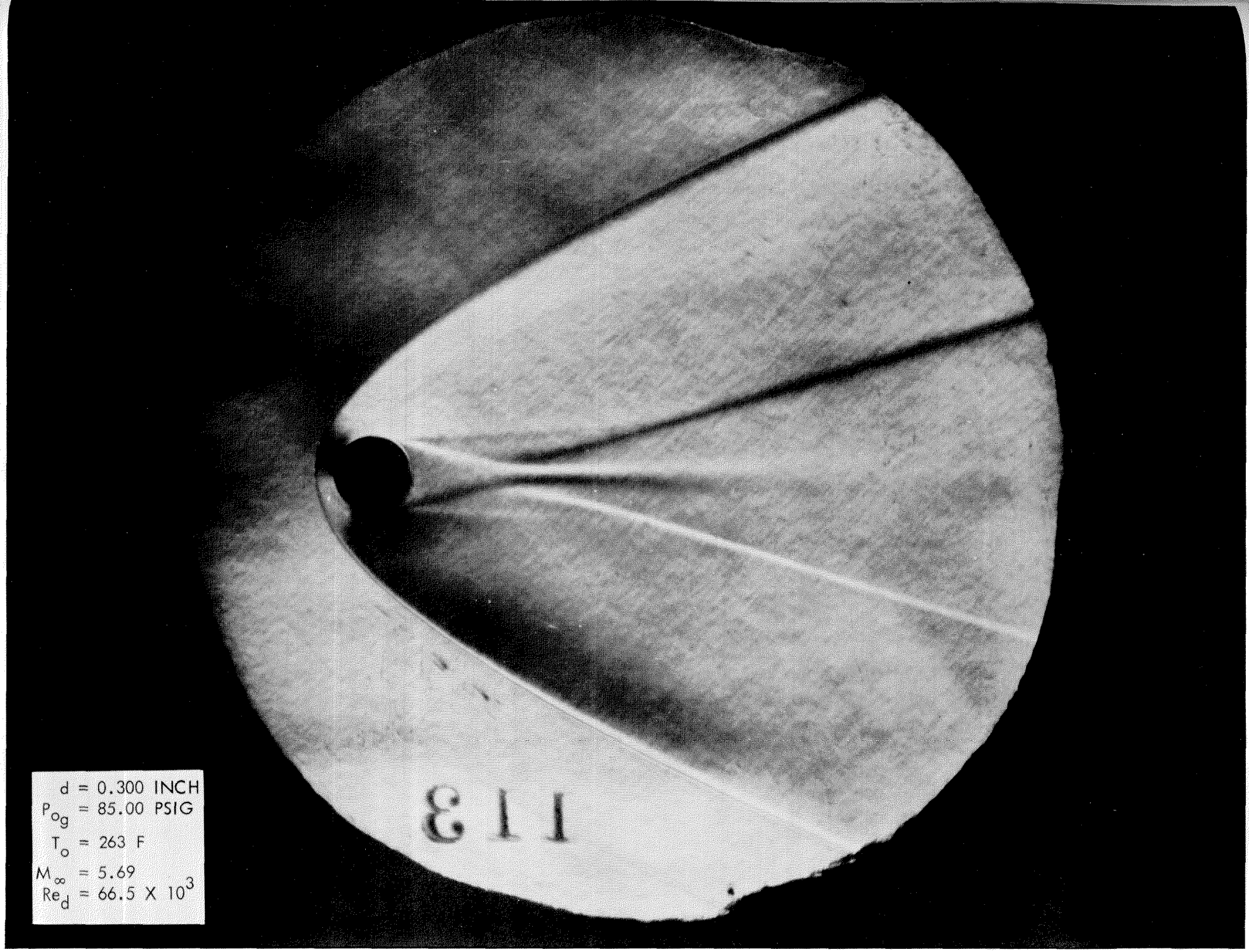

Figure 1. Schlieren Photograph of the Flow Around Cylinder

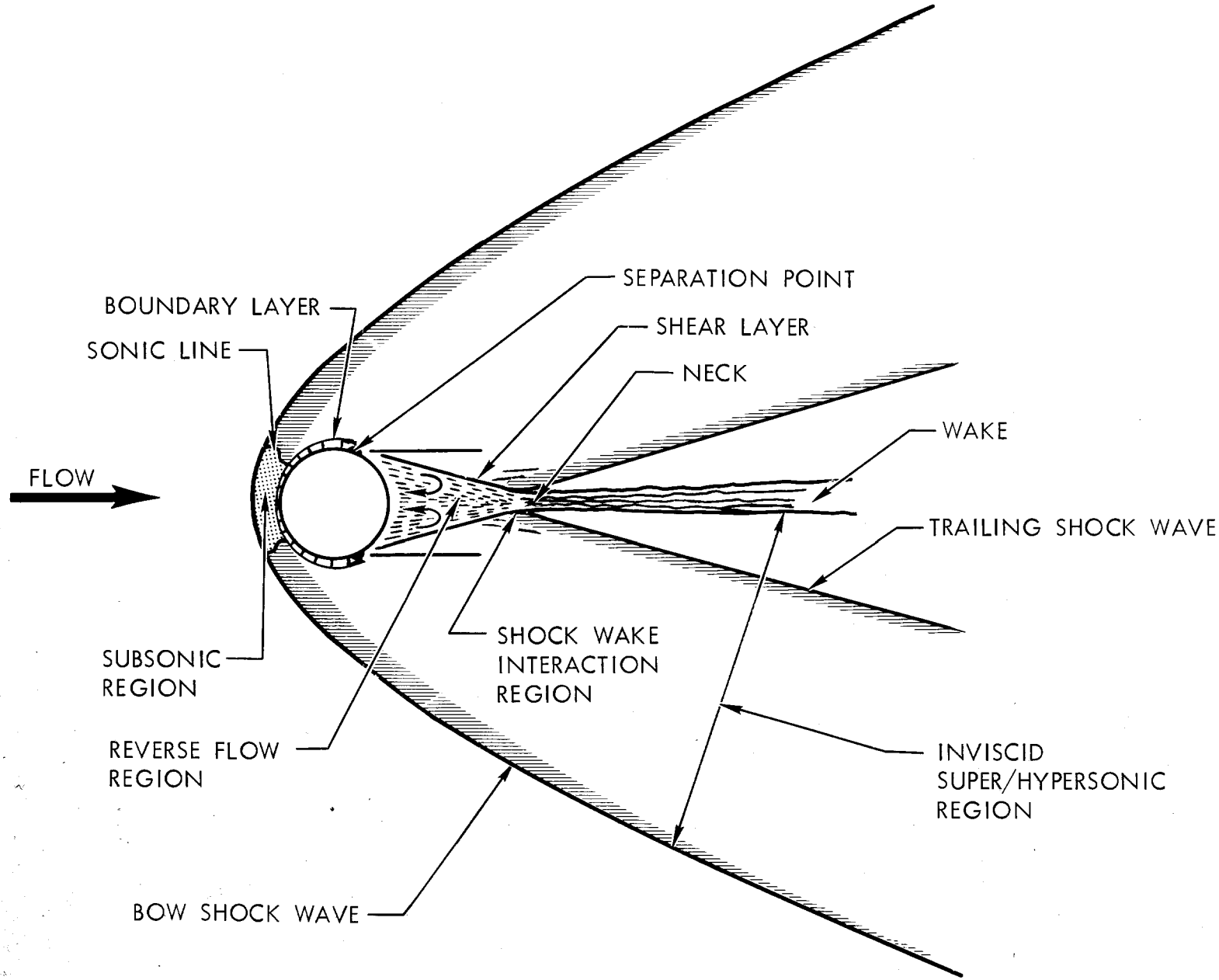

Figure 2. The Flow Field to be Analyzed

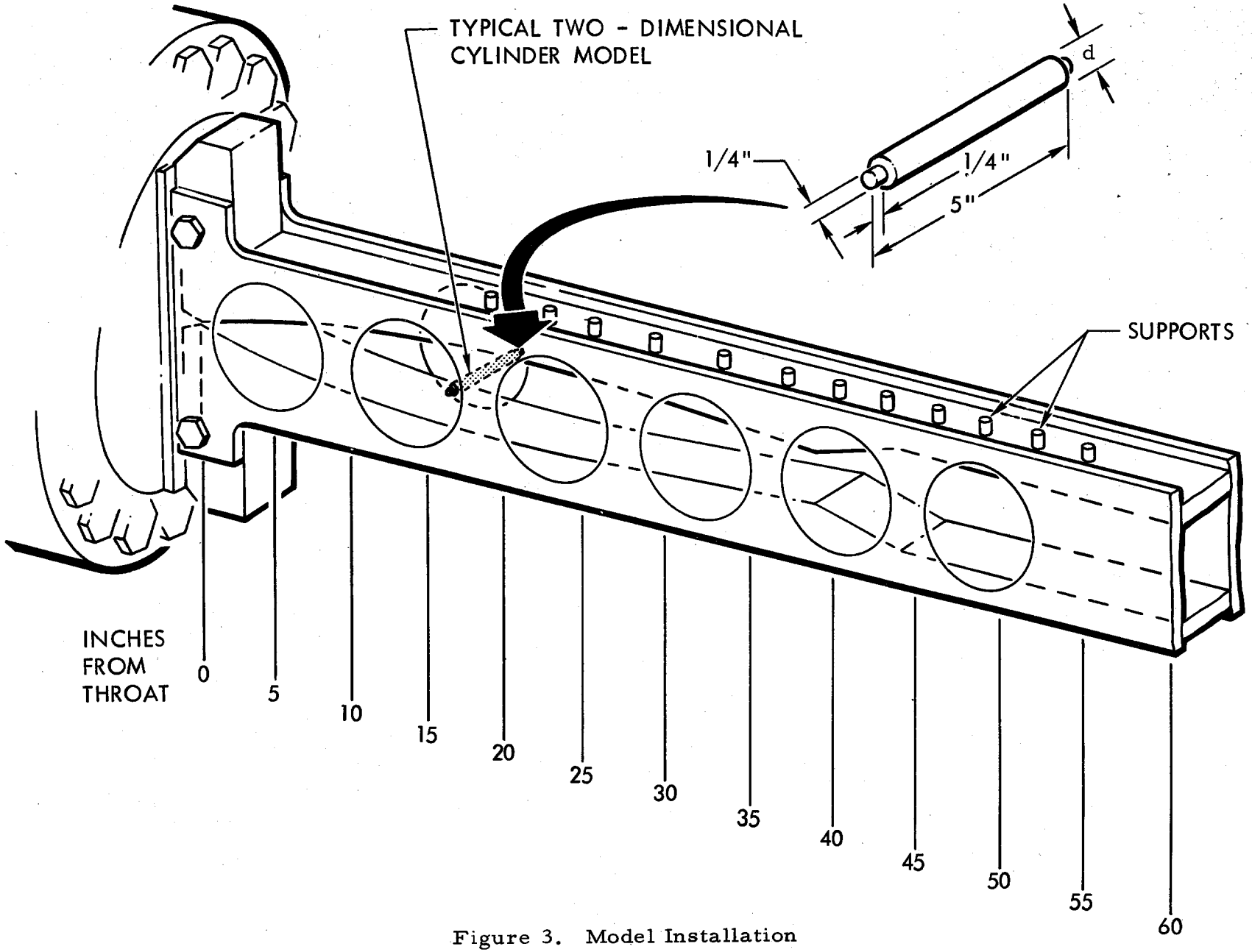

Figure 3. Model Installation

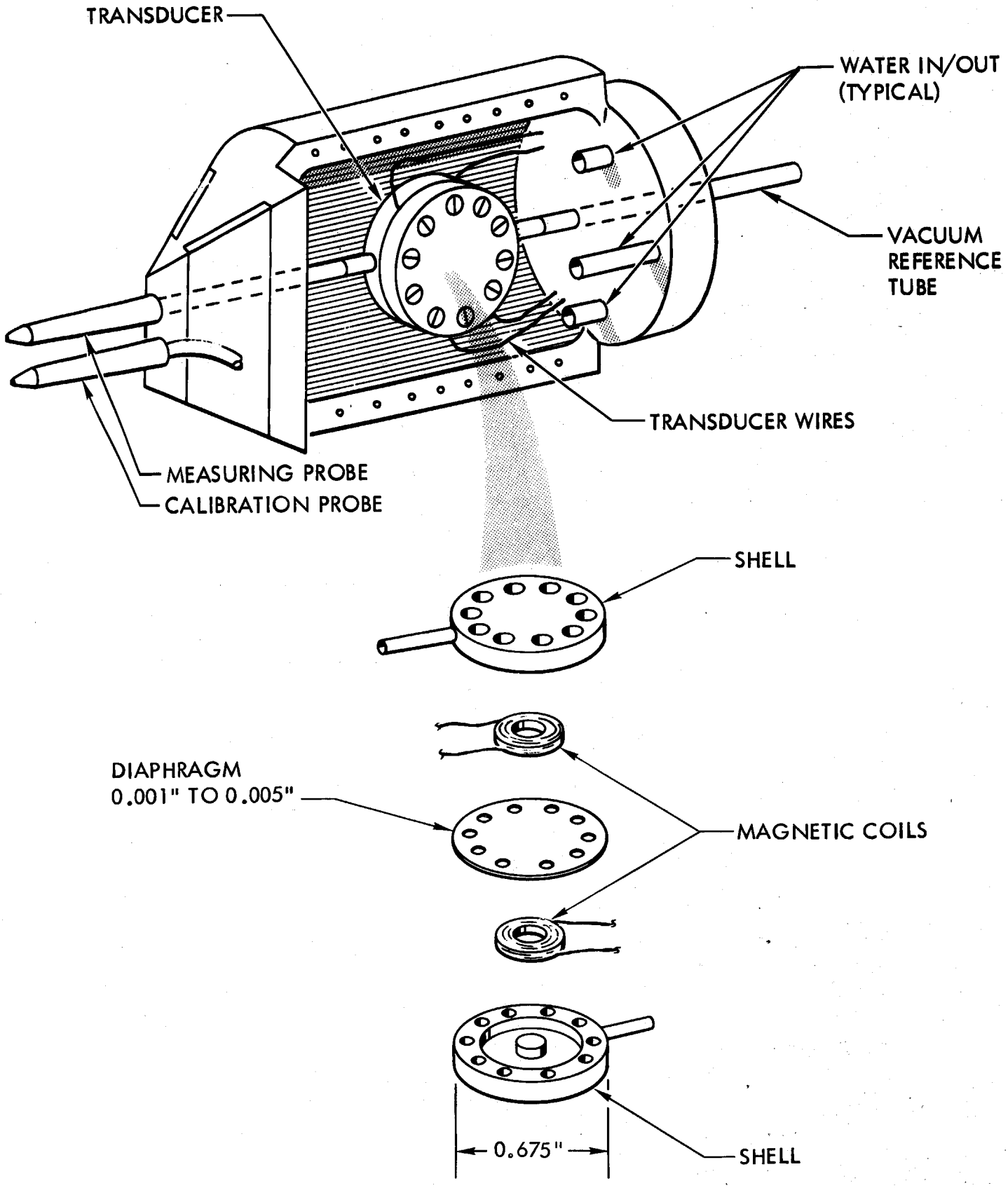

Figure 4. Installation of Variable-Reluctance Pressure Transducer

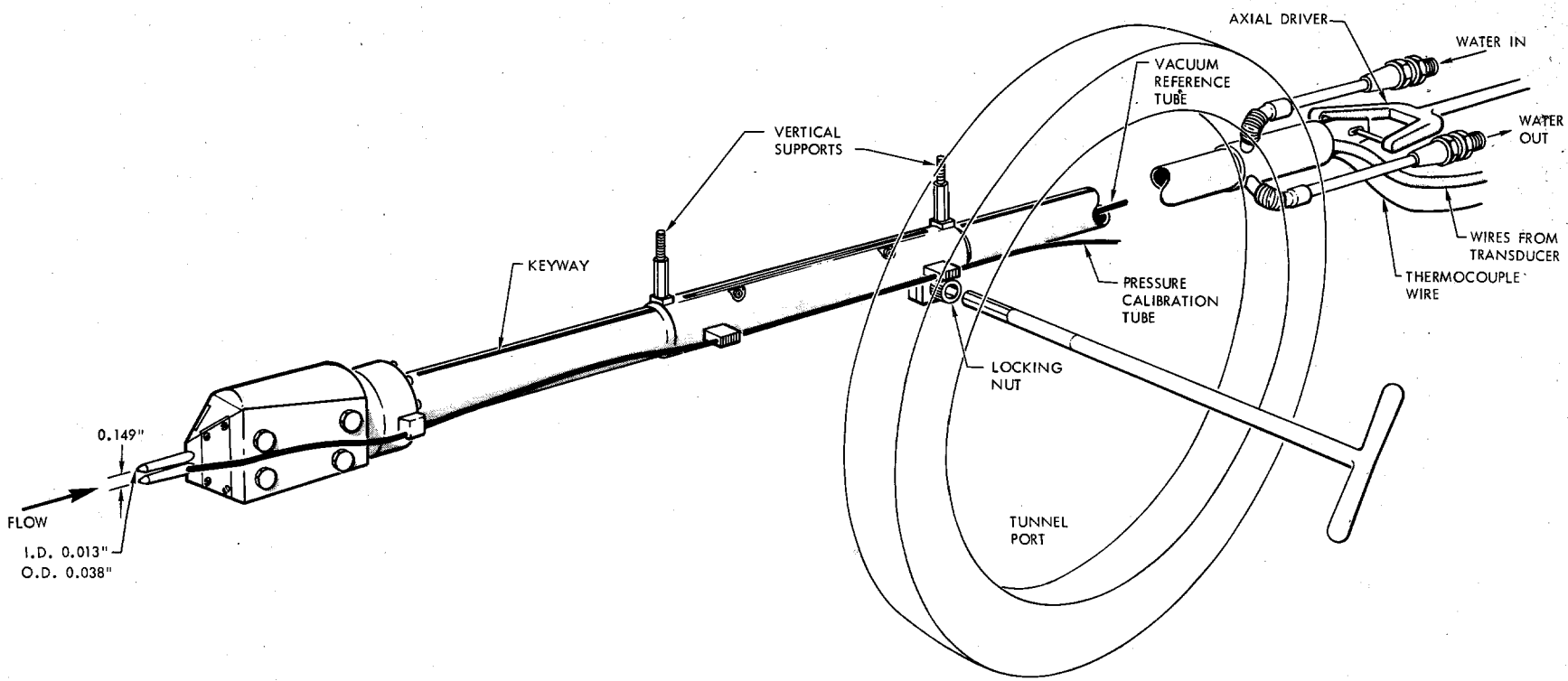

Figure 5. Pitot-Pressure Probe

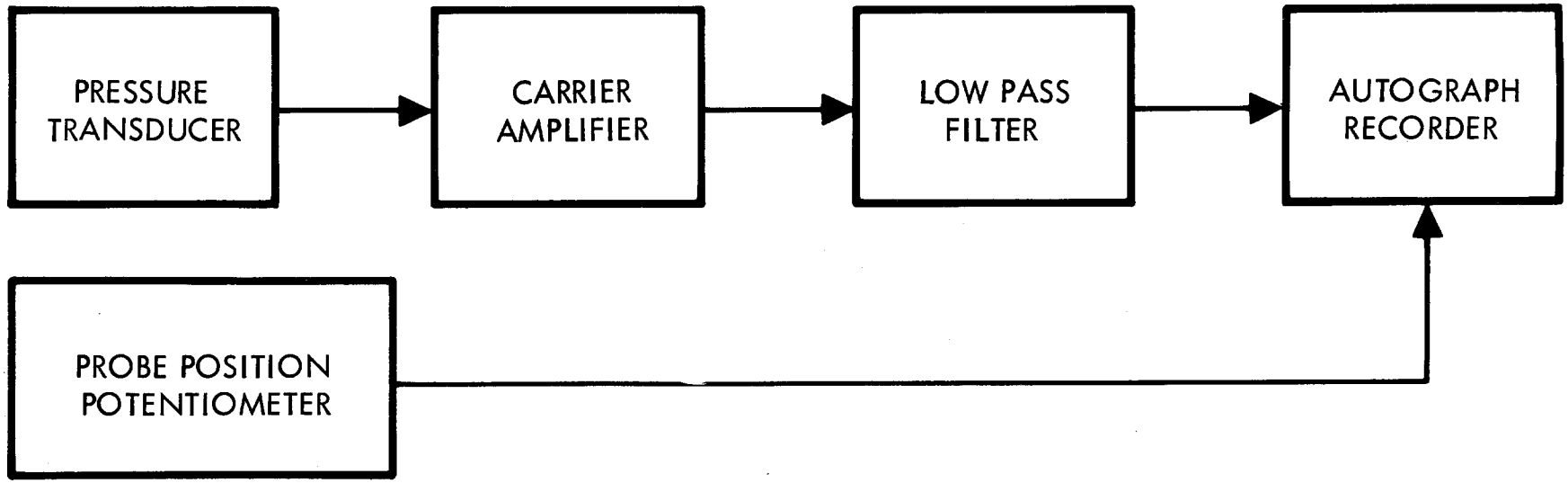

Figure 6. Pressure Recording System

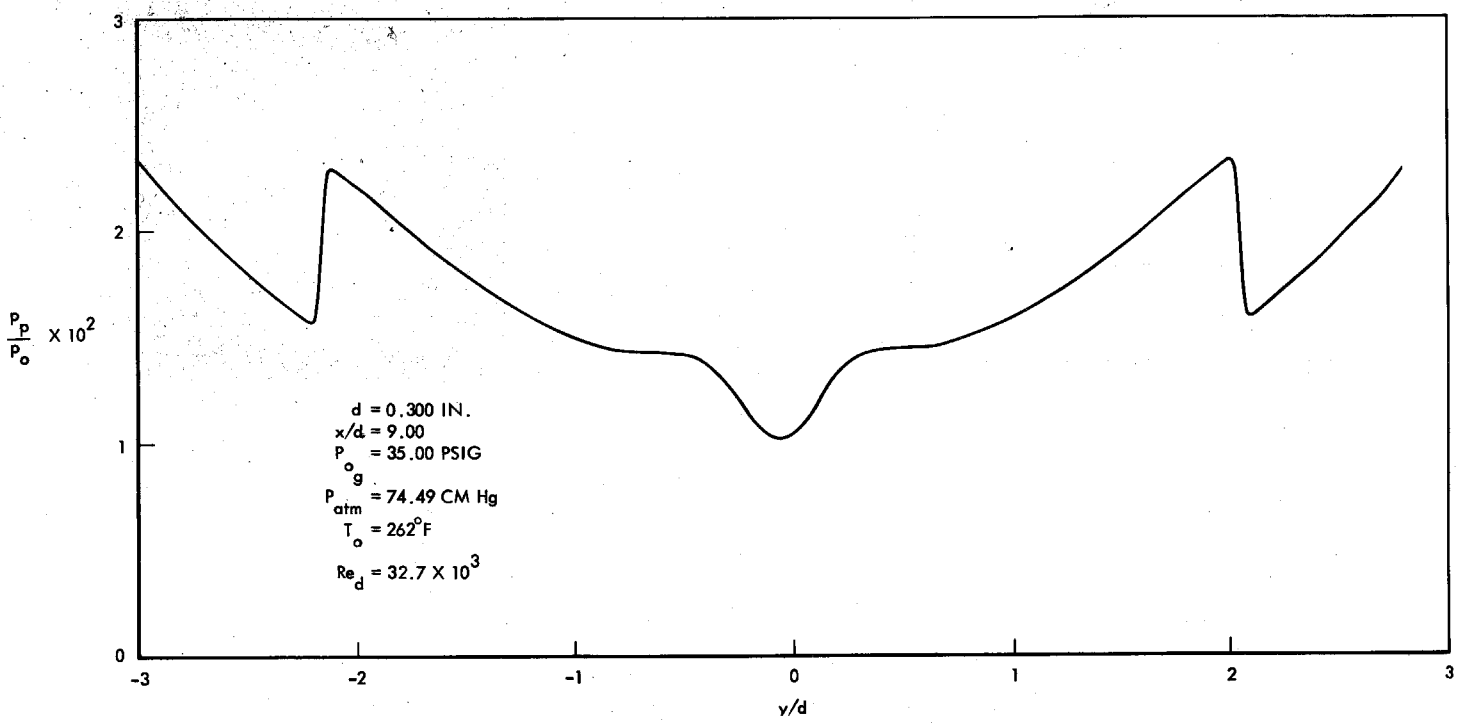

(a) Laminar Flow

Figure 7. Typical Pitot-Pressure Traces

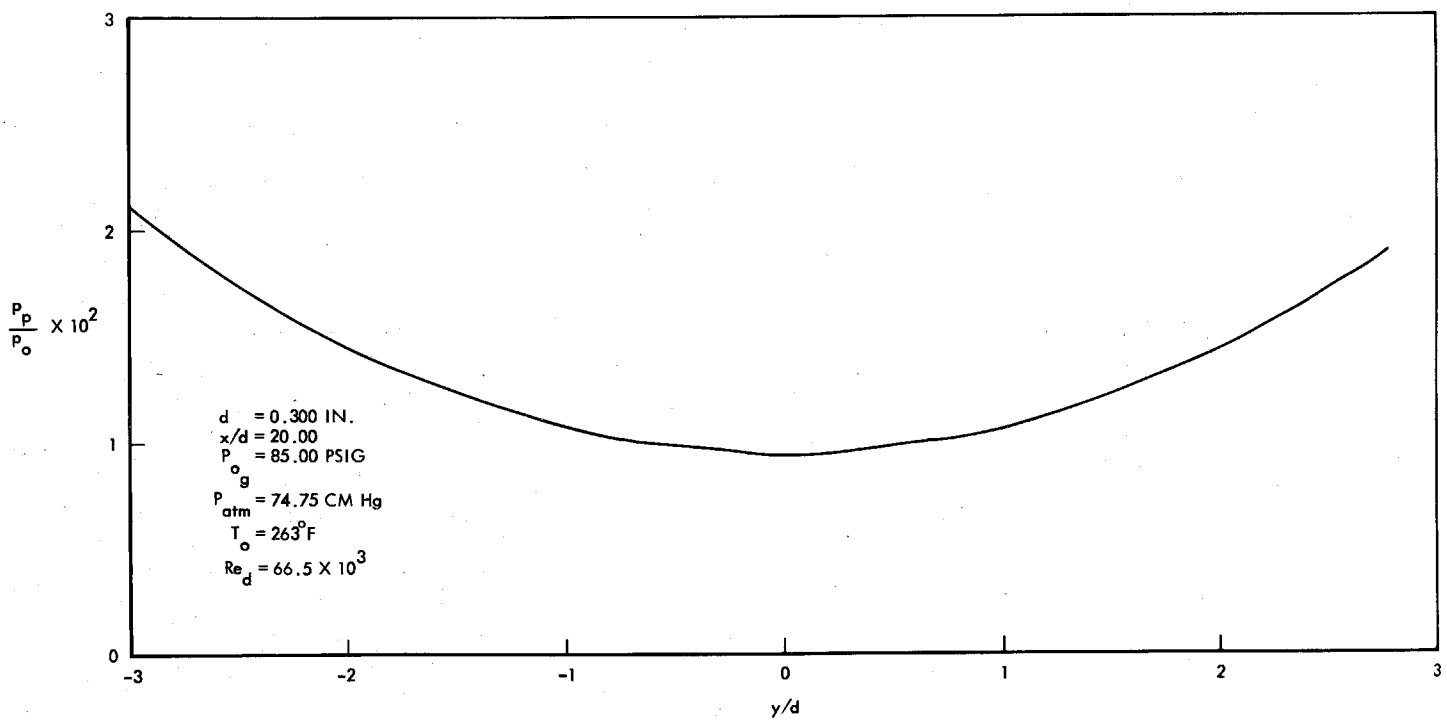

(b) Turbulent Flow

Figure 7. Typical Pitot-Pressure Traces

Model: d = 0.300 inch
p_{o_g} = 85.00 psig
p_{atm} = 74.69 cm Hg
T_o = 263 F
M_∞ = 5.69
Re_d = 66.5 x 10^3

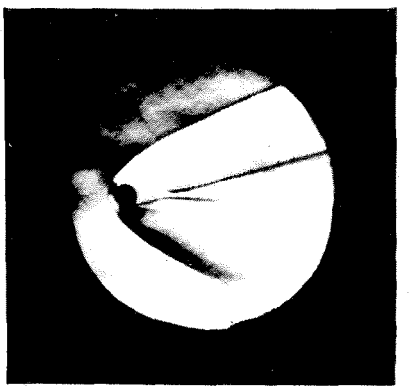

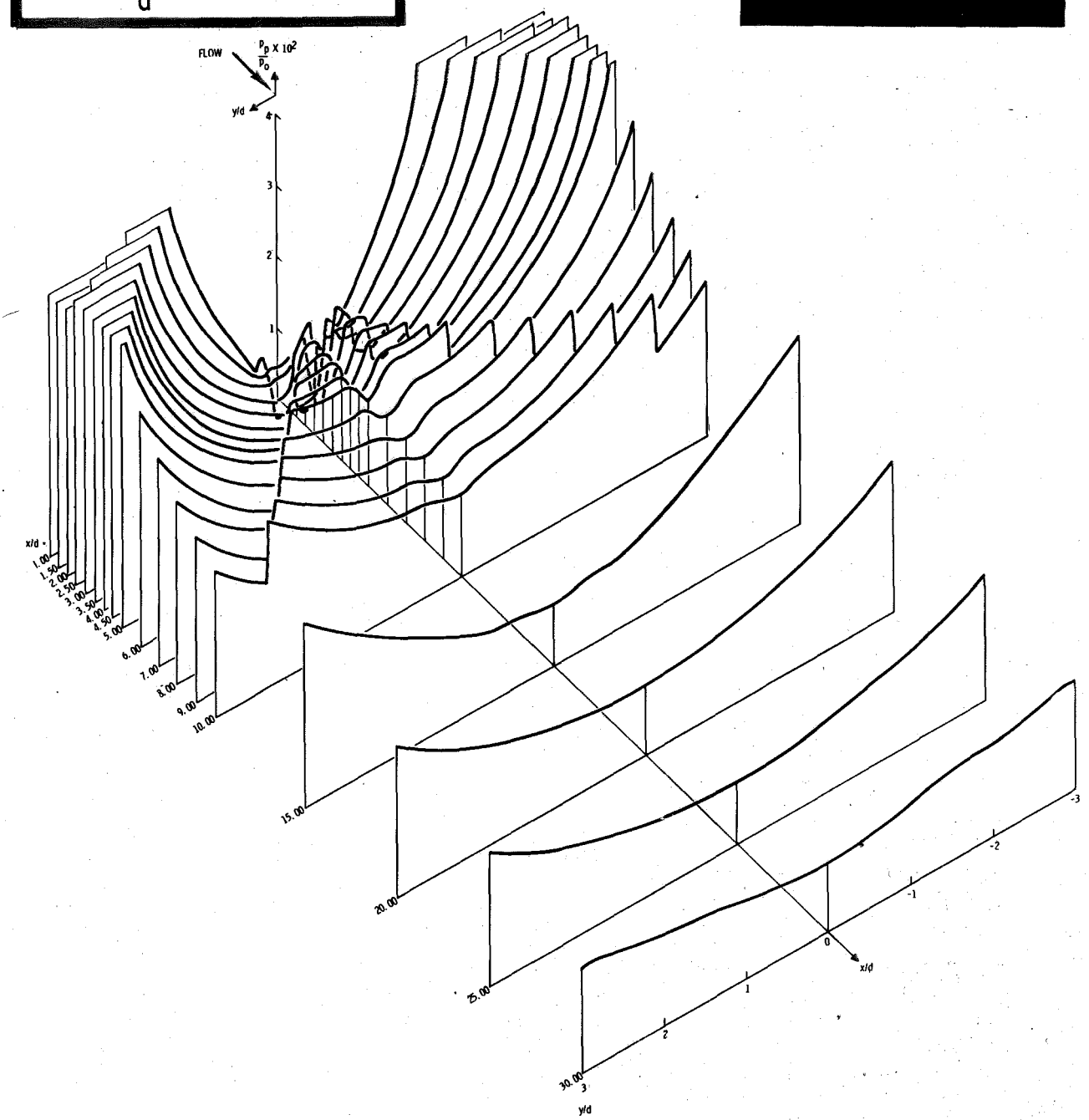

Figure 8. Isoaxiometric Pitot-Pressure Traces

Model: d = 0.300 inch
p_{o_g} = 85.00 psig
p_{atm} = 74.69 cm Hg
T_o = 263 F
M_∞ = 5.69
Re_d = 66.5 x 10^3

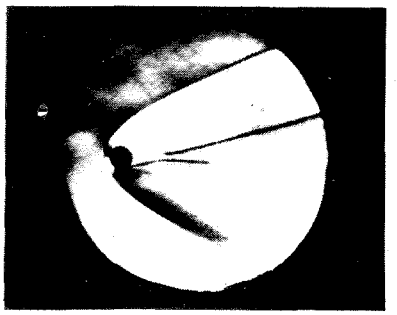

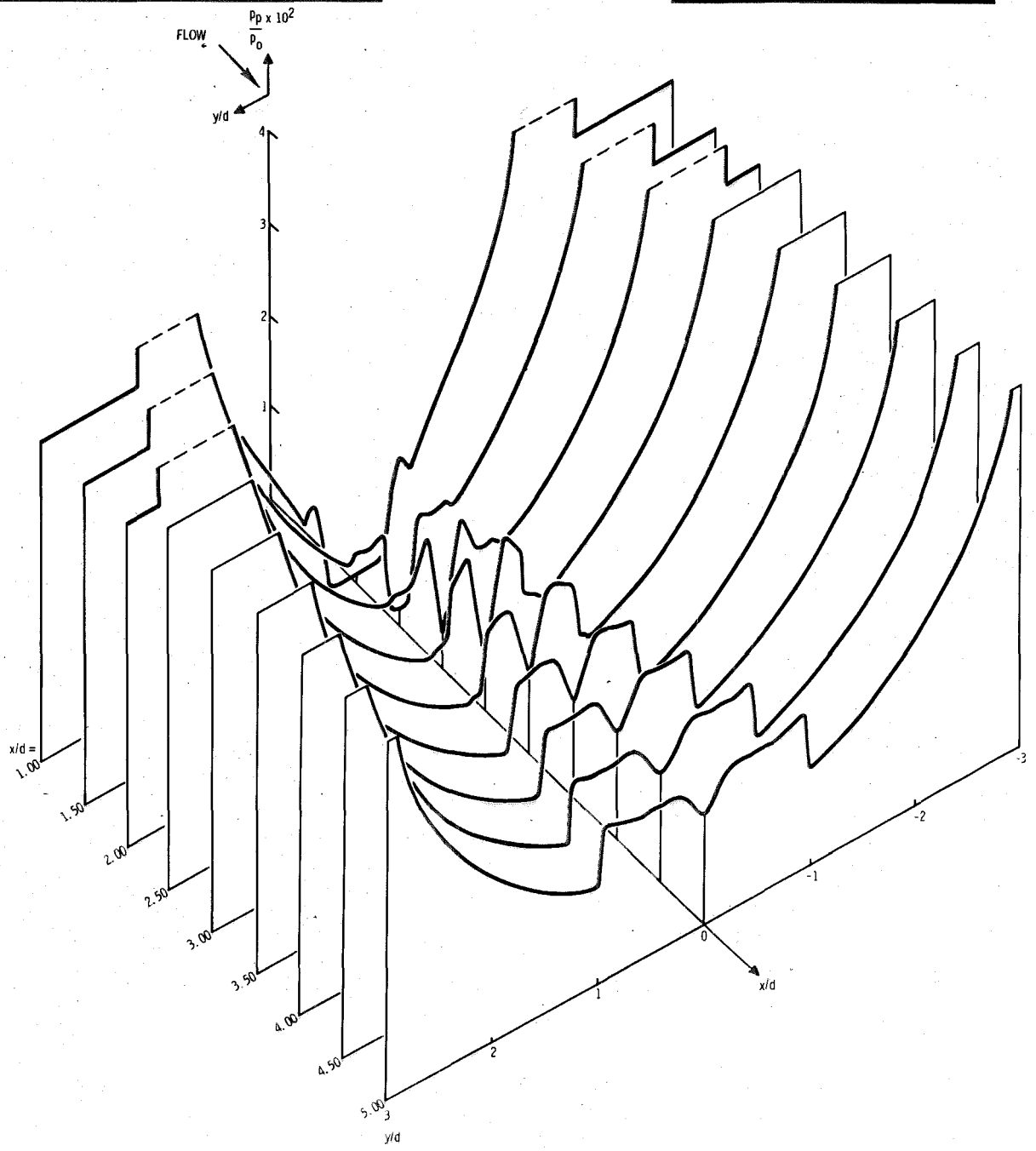

Figure 9. Isoaxiometric Pitot-Pressure Traces

Model: d = 0.300 inch
p_{o_g} = 10.00 psig
p_{atm} = 74.36 cm Hg
T_o = 262 F
M_∞ = 5.64
Re_d = 16.7 x 10^3

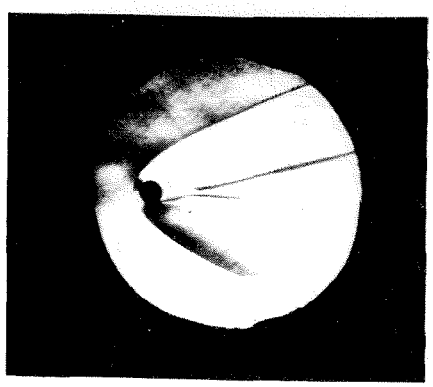

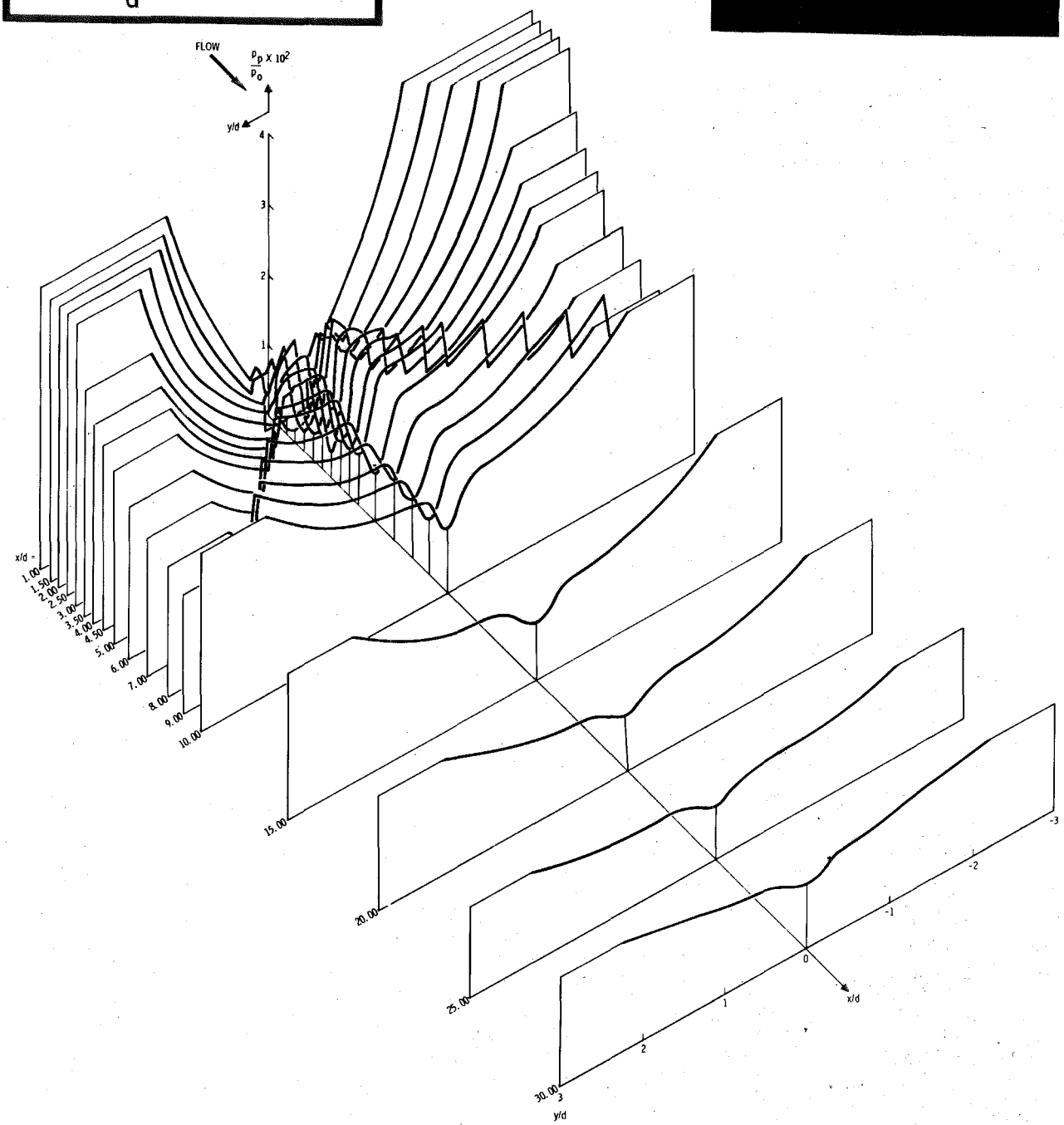

Figure 10. Isoaxiometric Pitot-Pressure Traces

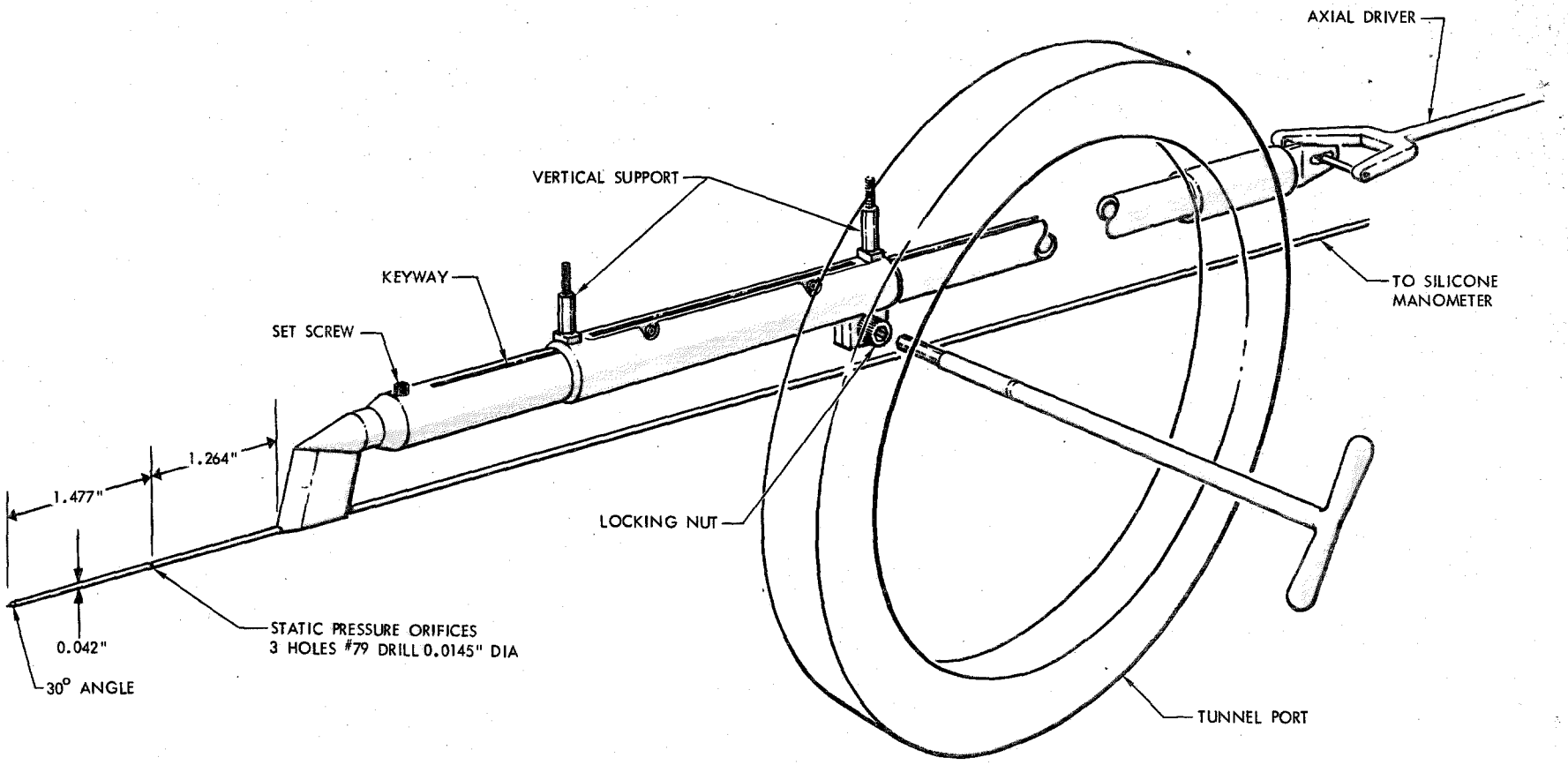

Figure 11. Static-Pressure Probe

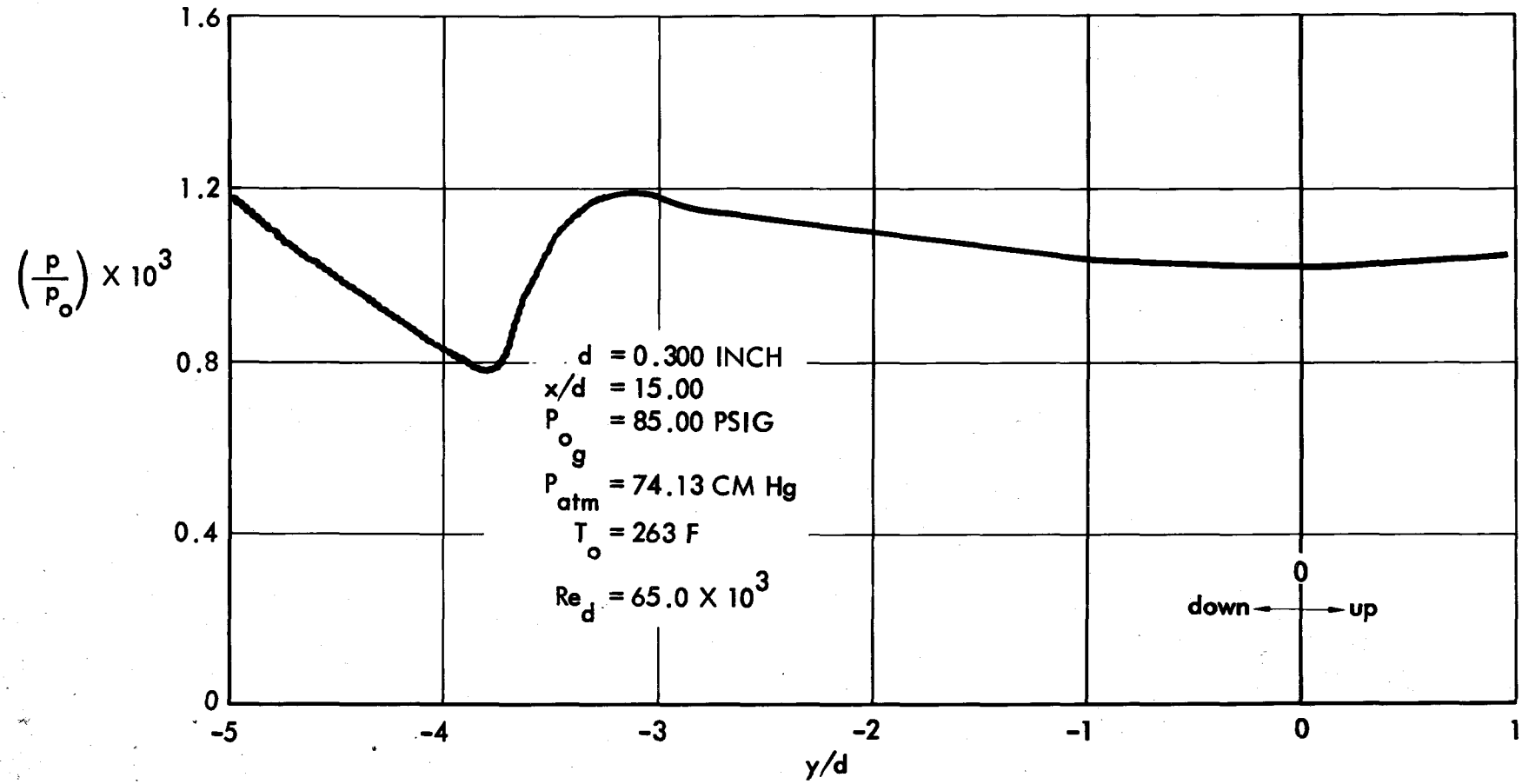

Figure 12. Typical Vertical Static-Pressure Survey

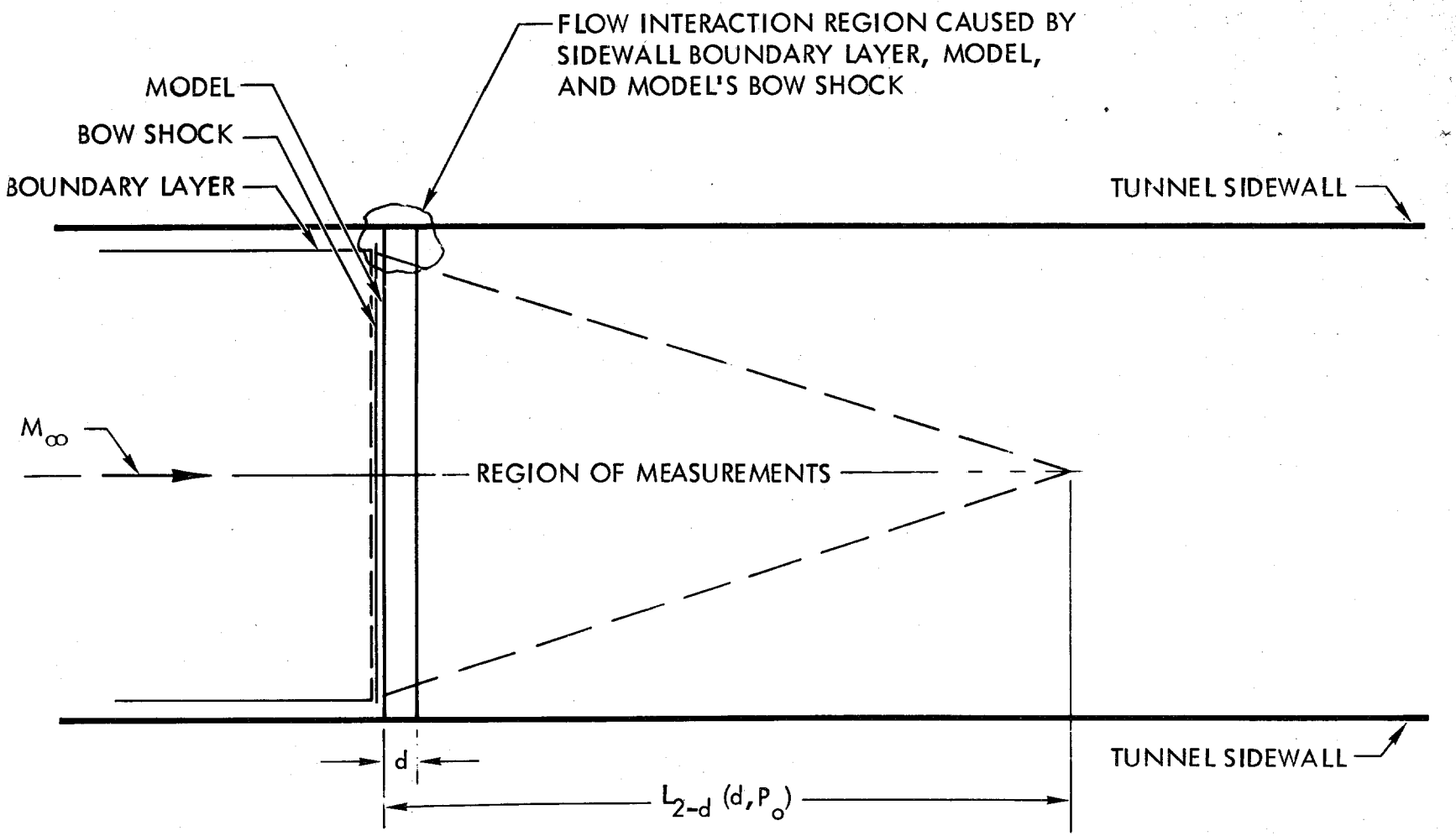

Figure 13. Two-Dimensional Region of Tests

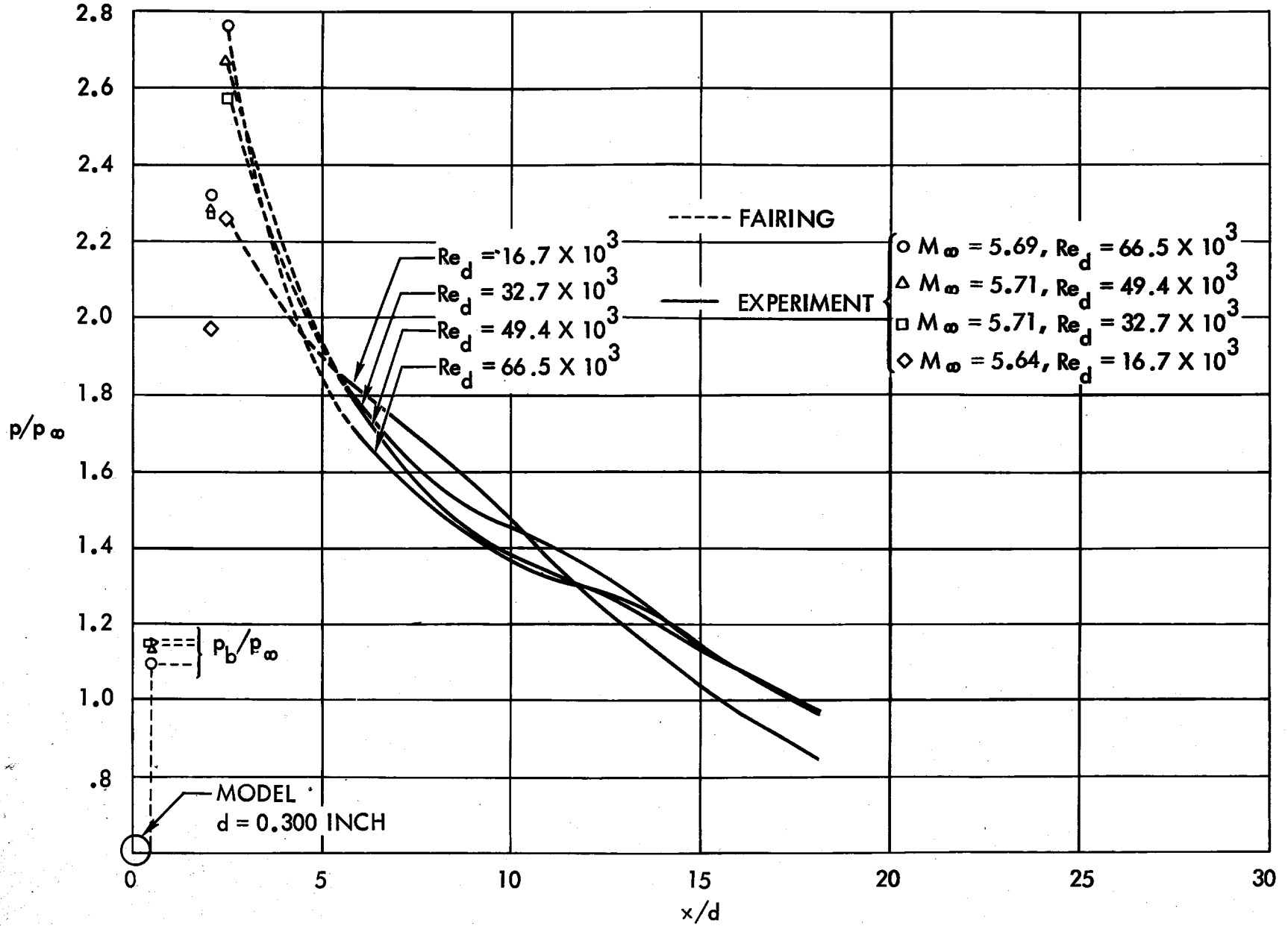

(a) 0.300-Inch Diameter Cylinder

Figure 14. Axial Static-Pressure Traces

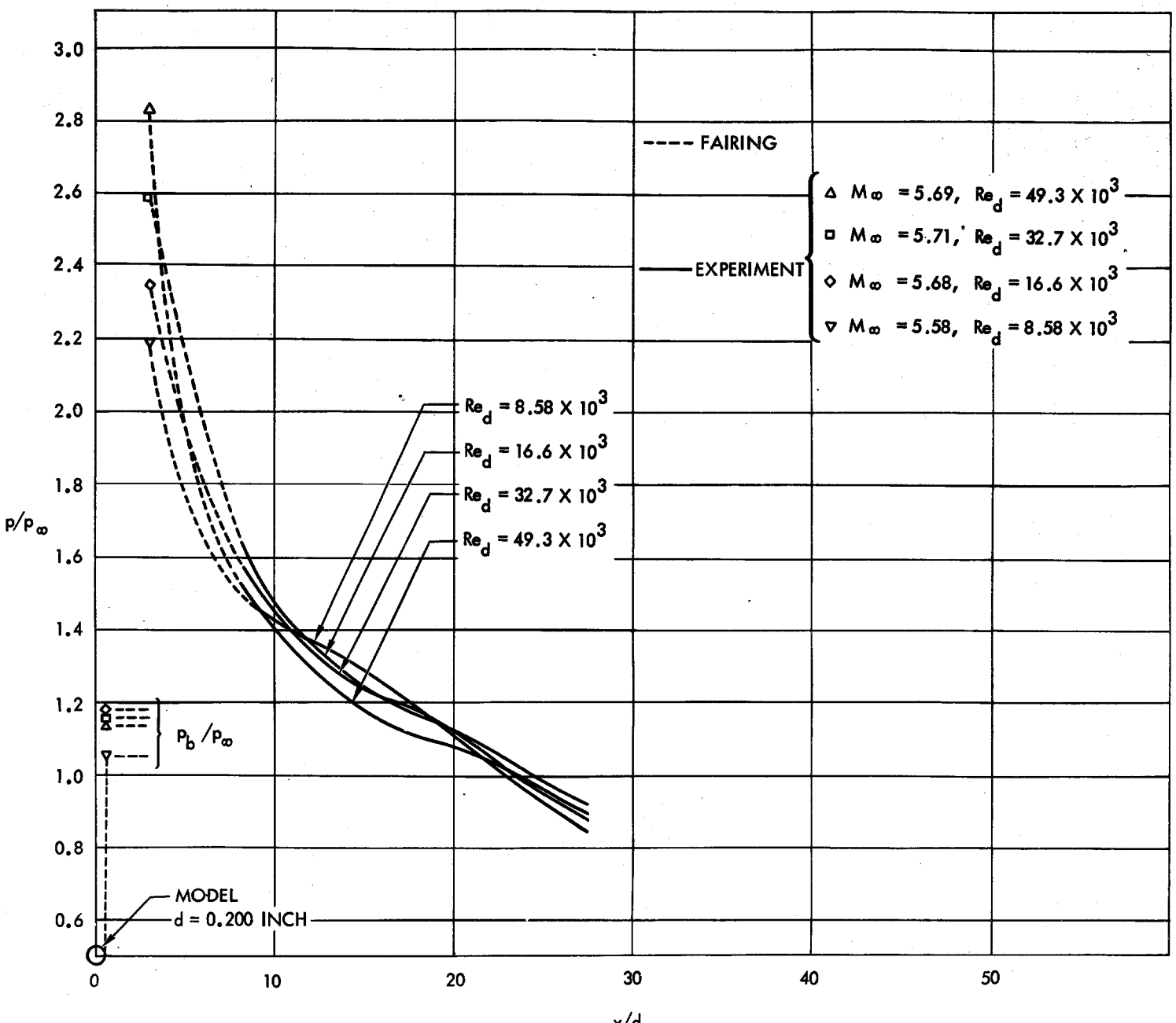

(b) 0.200-Inch Diameter Cylinder

Figure 14. Axial Static-Pressure Traces

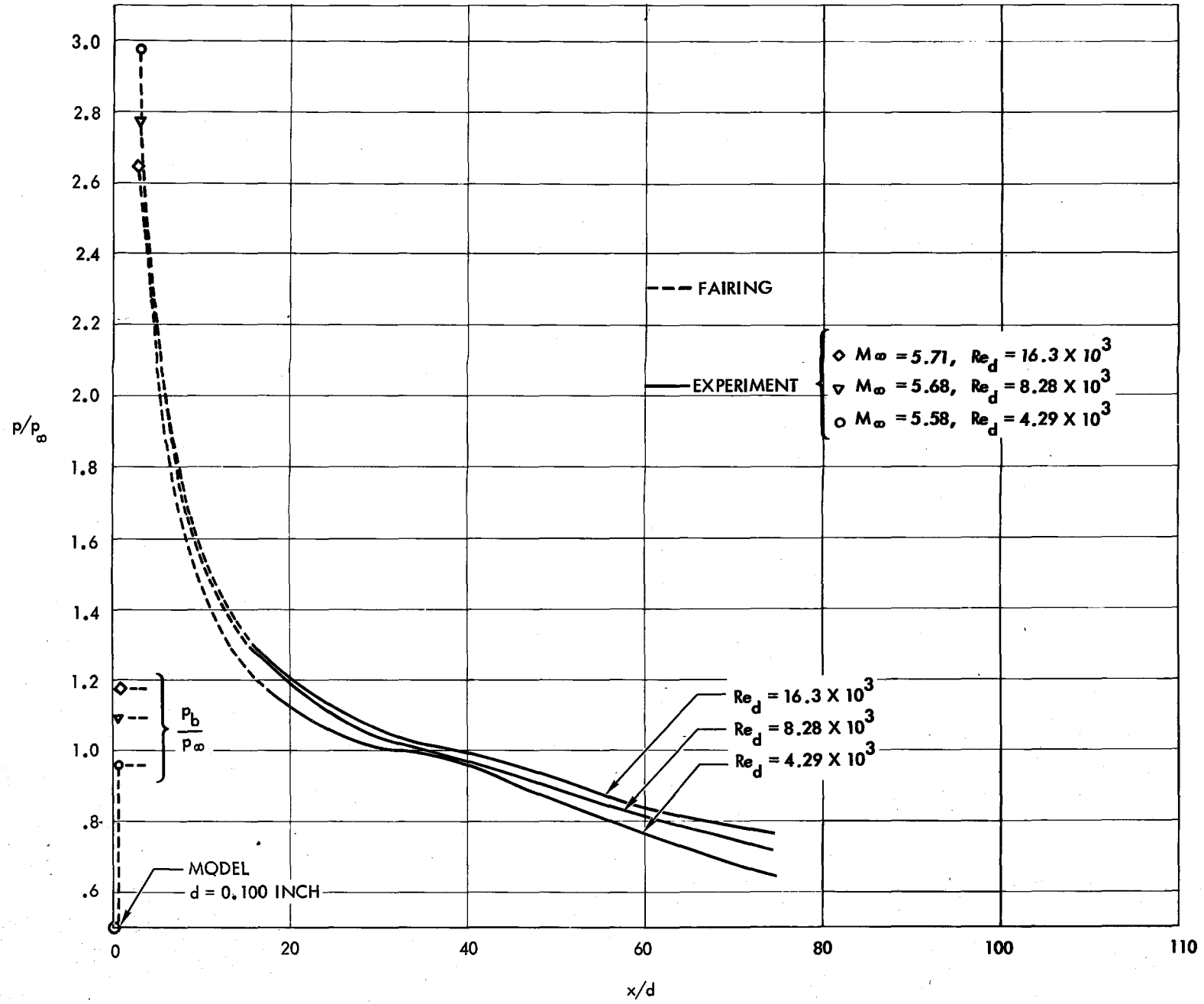

(c) 0.100-Inch Diameter Cylinder

Figure 14. Axial Static-Pressure Traces

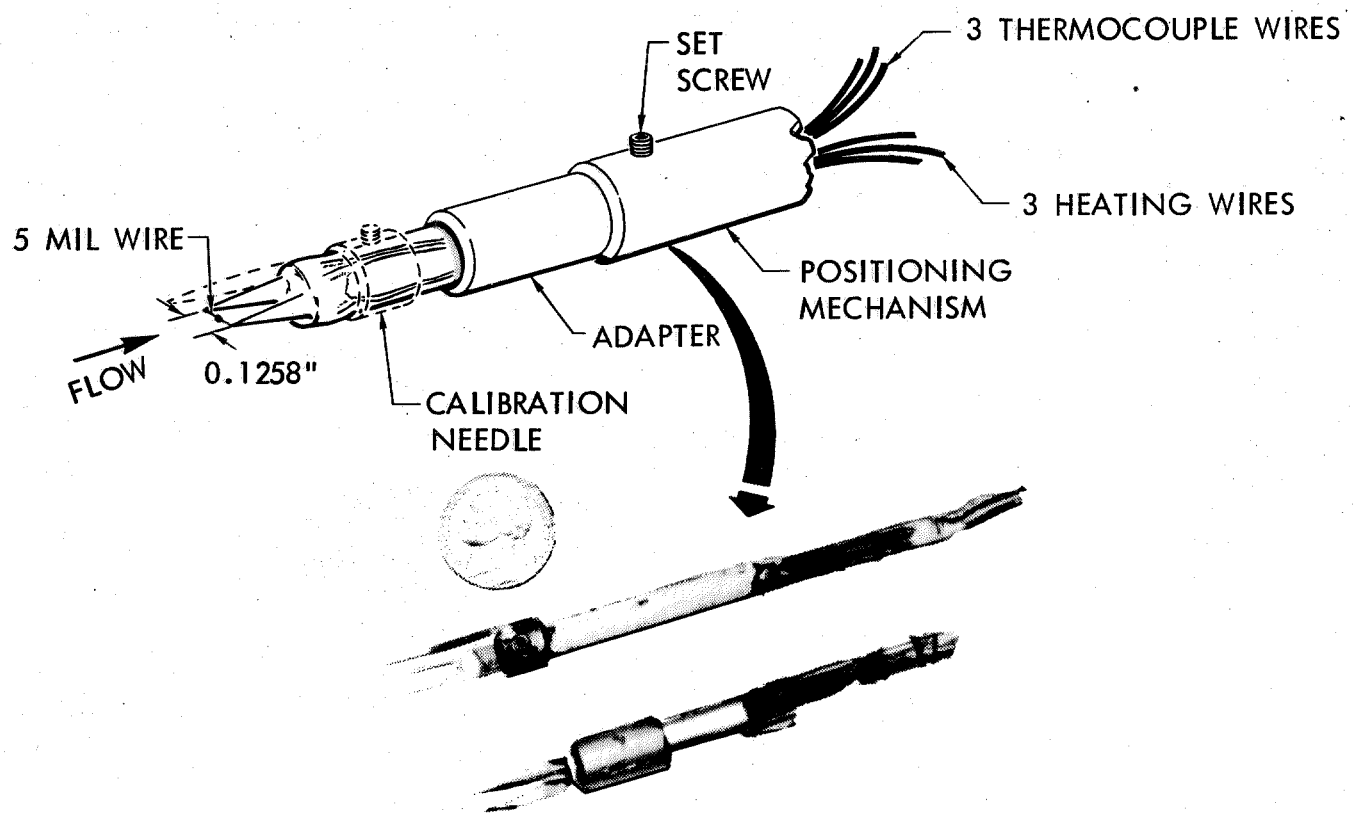

Figure 15. Heated Thermocouple

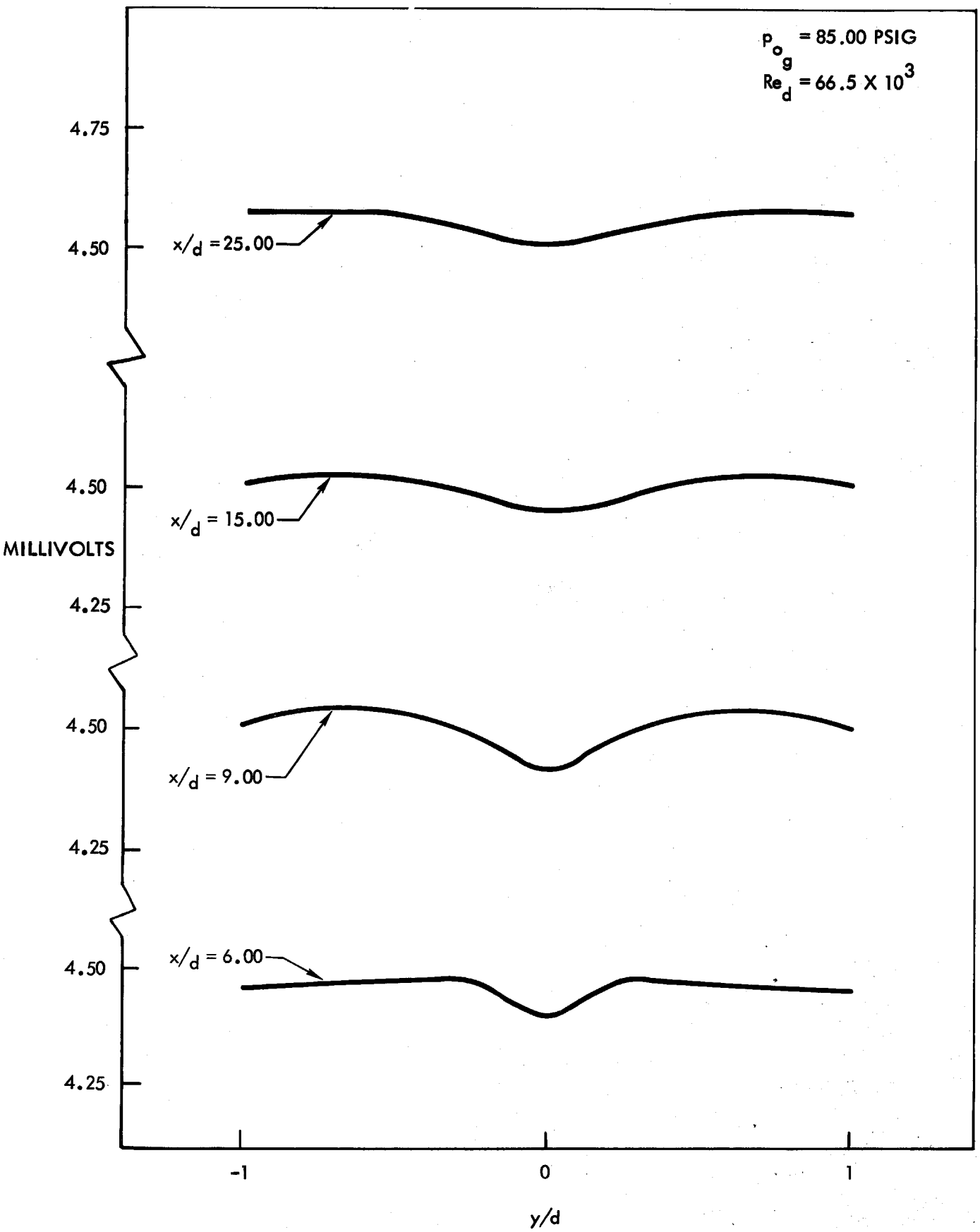

(a) p_{o_g} = 85.00 psig

Figure 16. Total—Temperature Surveys

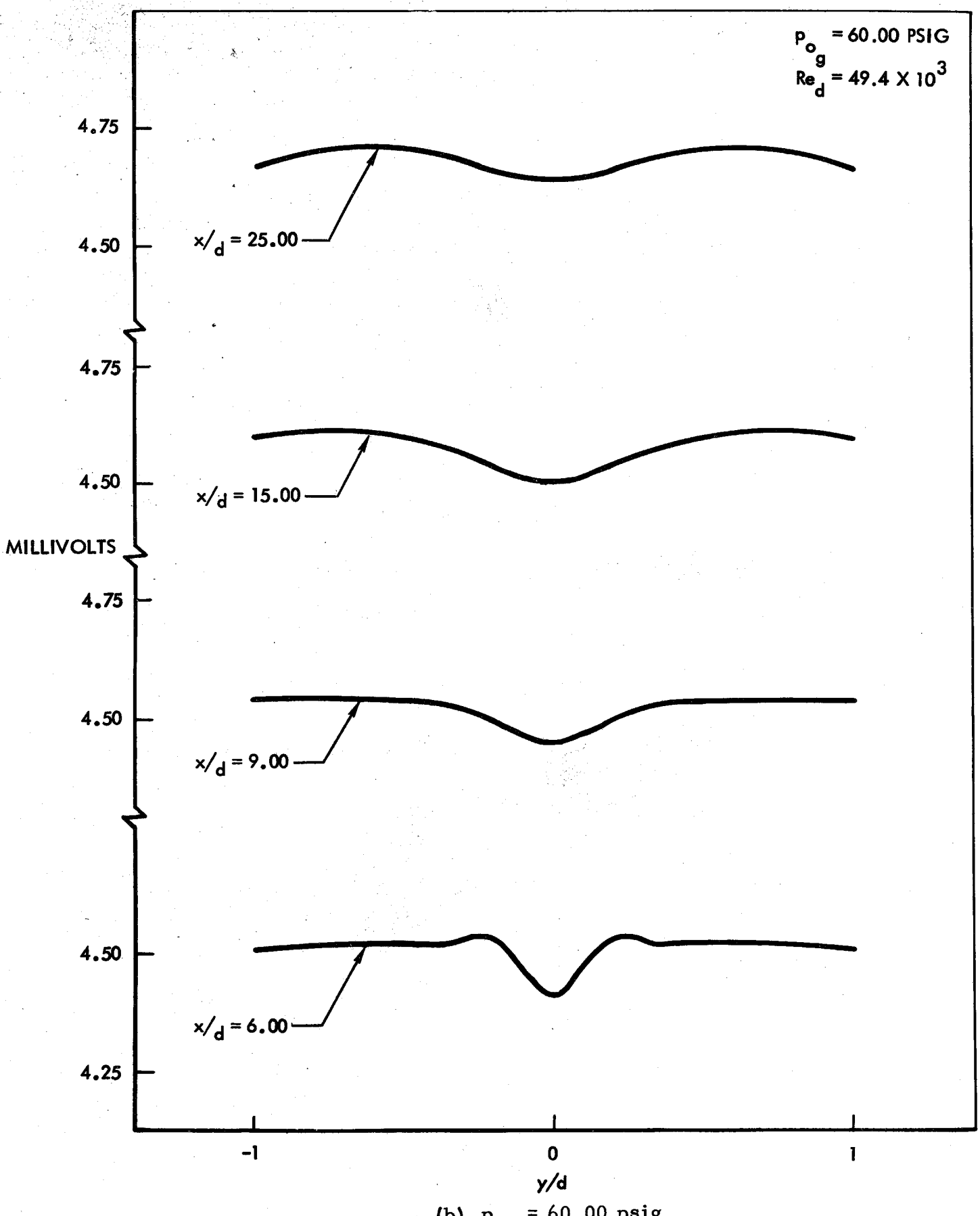

(b) p_{o_g} = 60.00 psig

Figure 16. Total—Temperature Surveys

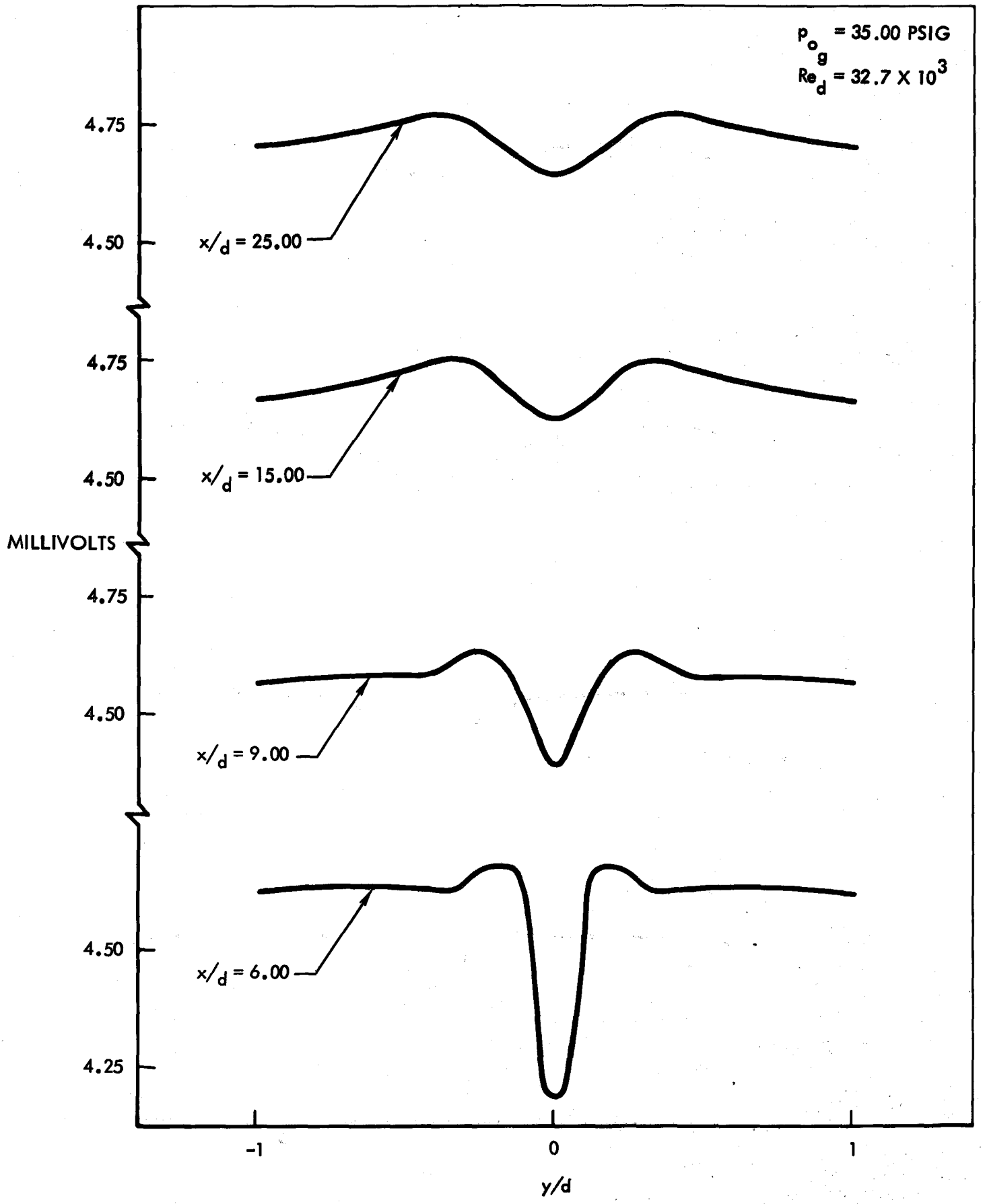

(c) p_{o_g} = 35.00 psig

Figure 16. Total—Temperature Surveys

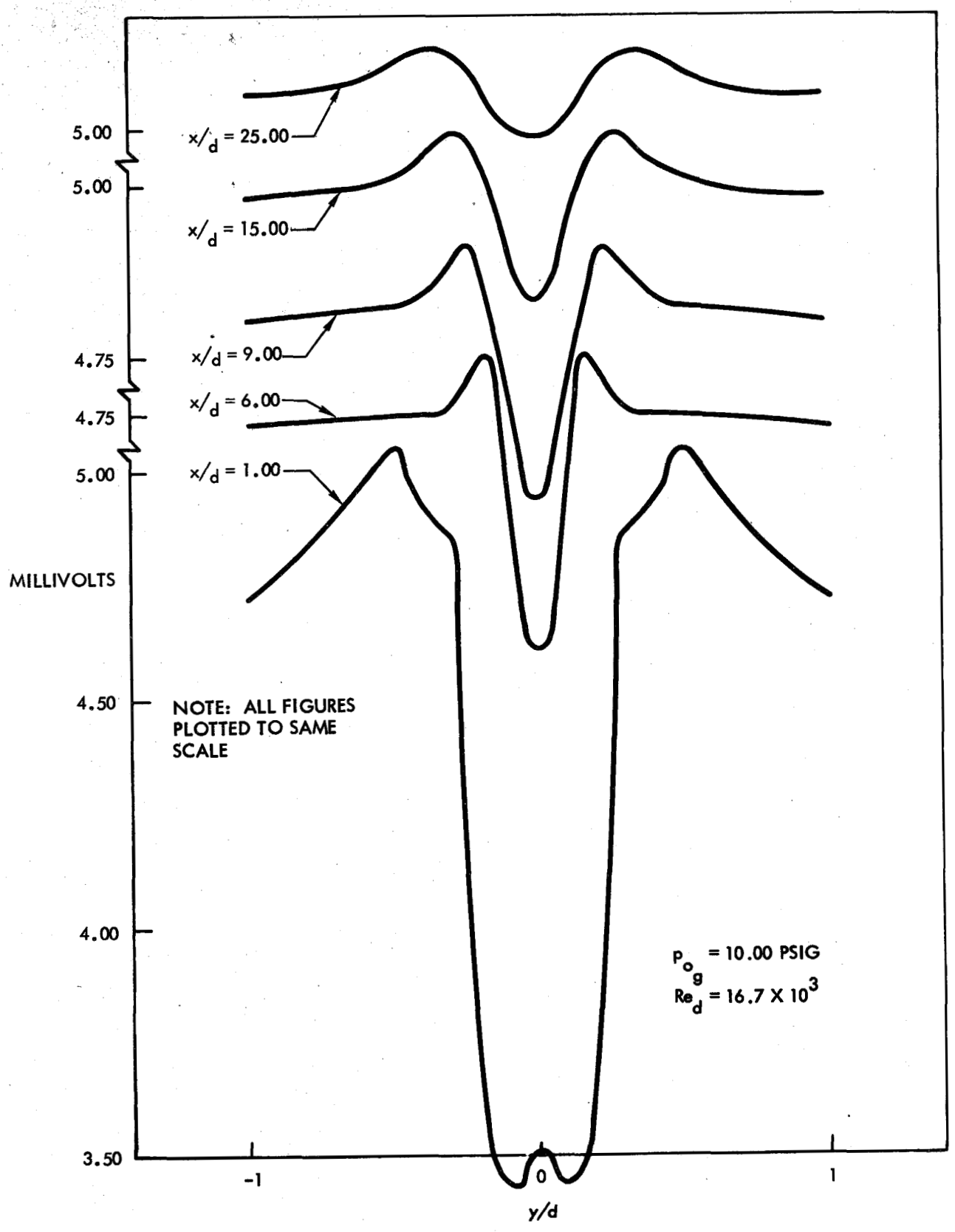

(d) p_{o_g} = 10.00 psig

Figure 16. Total—Temperature Surveys

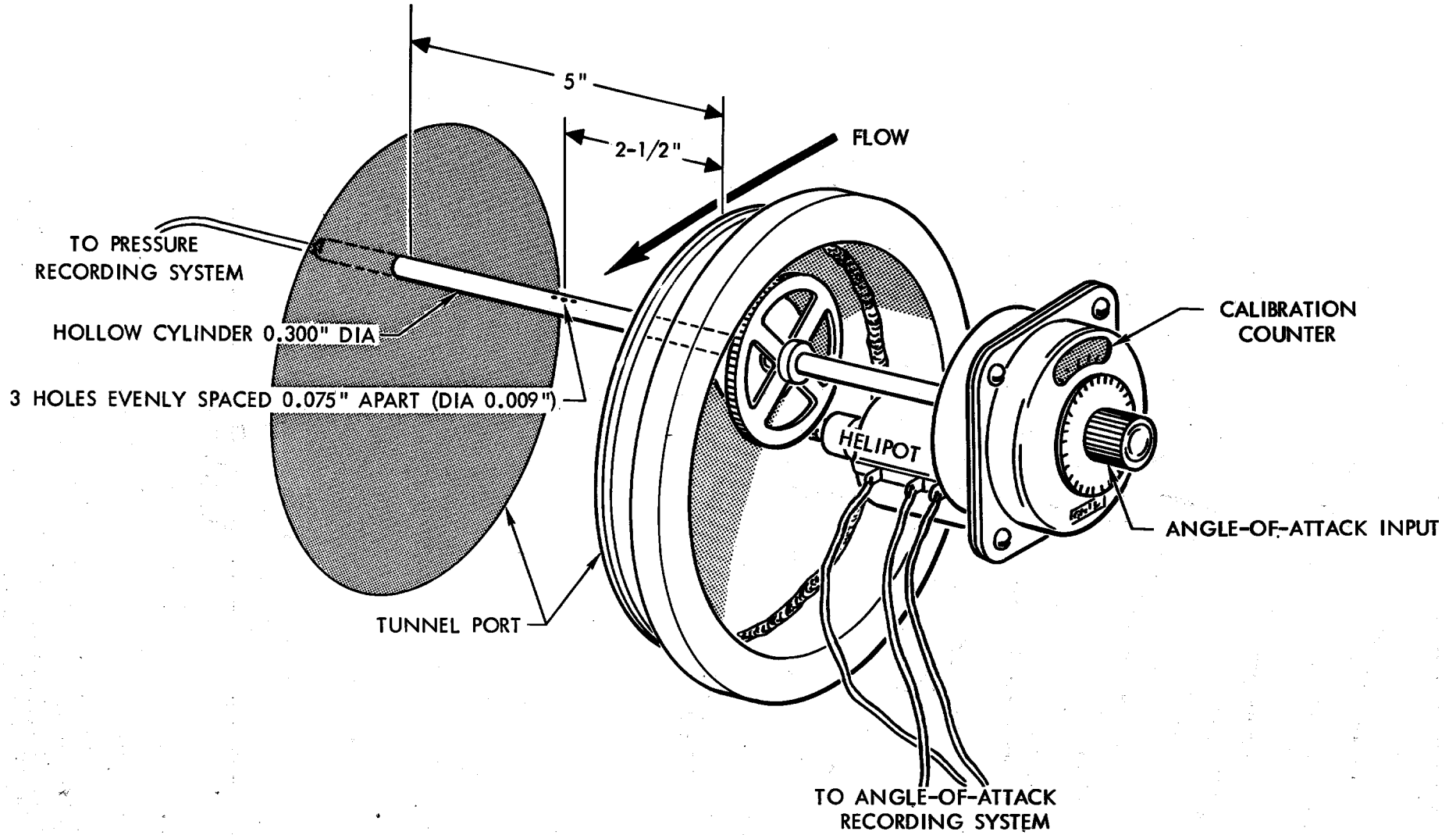

Figure 17. Apparatus for Measuring Base Pressure

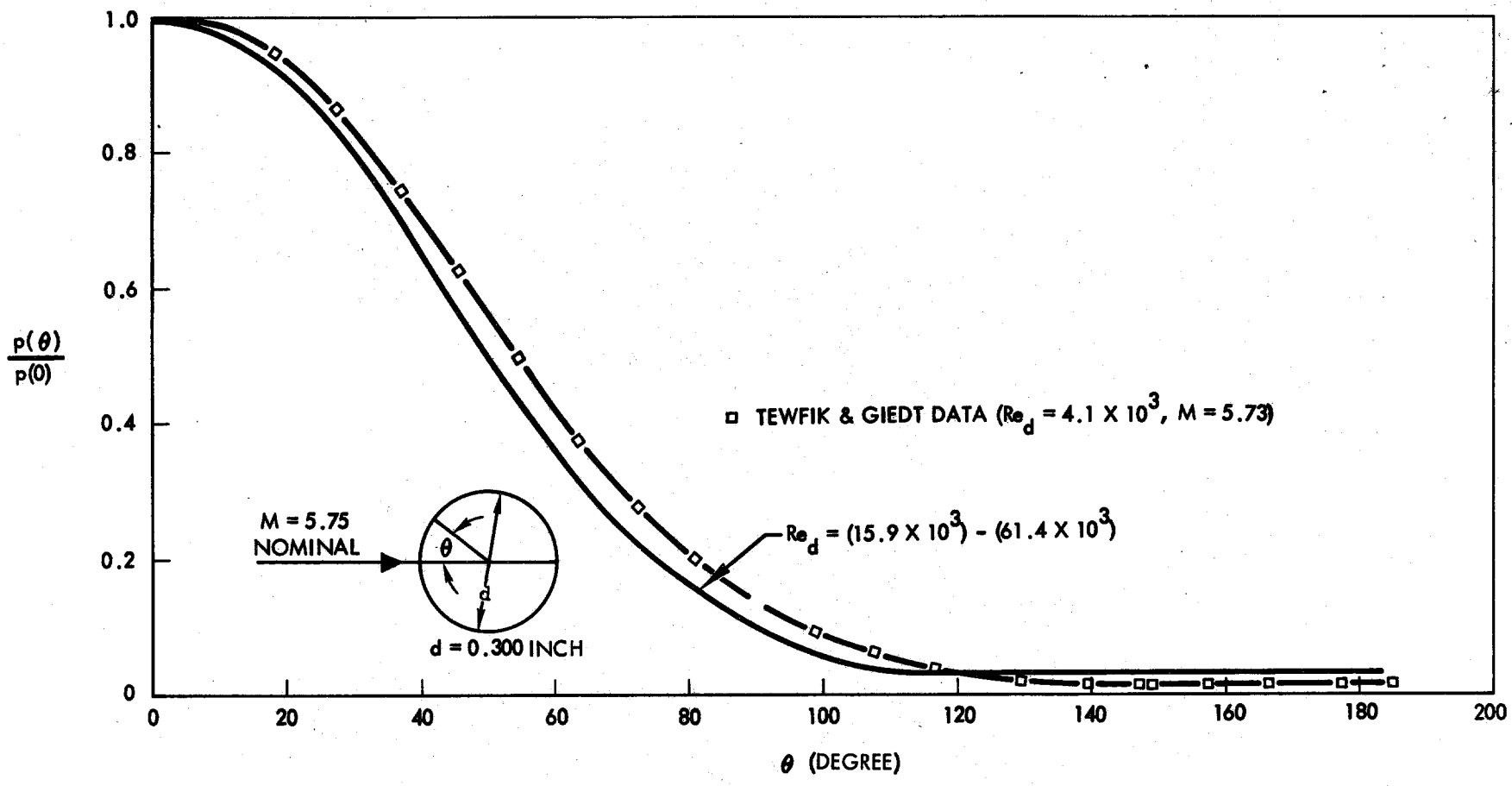

(a) Pressure Distribution on Cylinder

Figure 18. Experimental Pressure Distribution on Cylinder

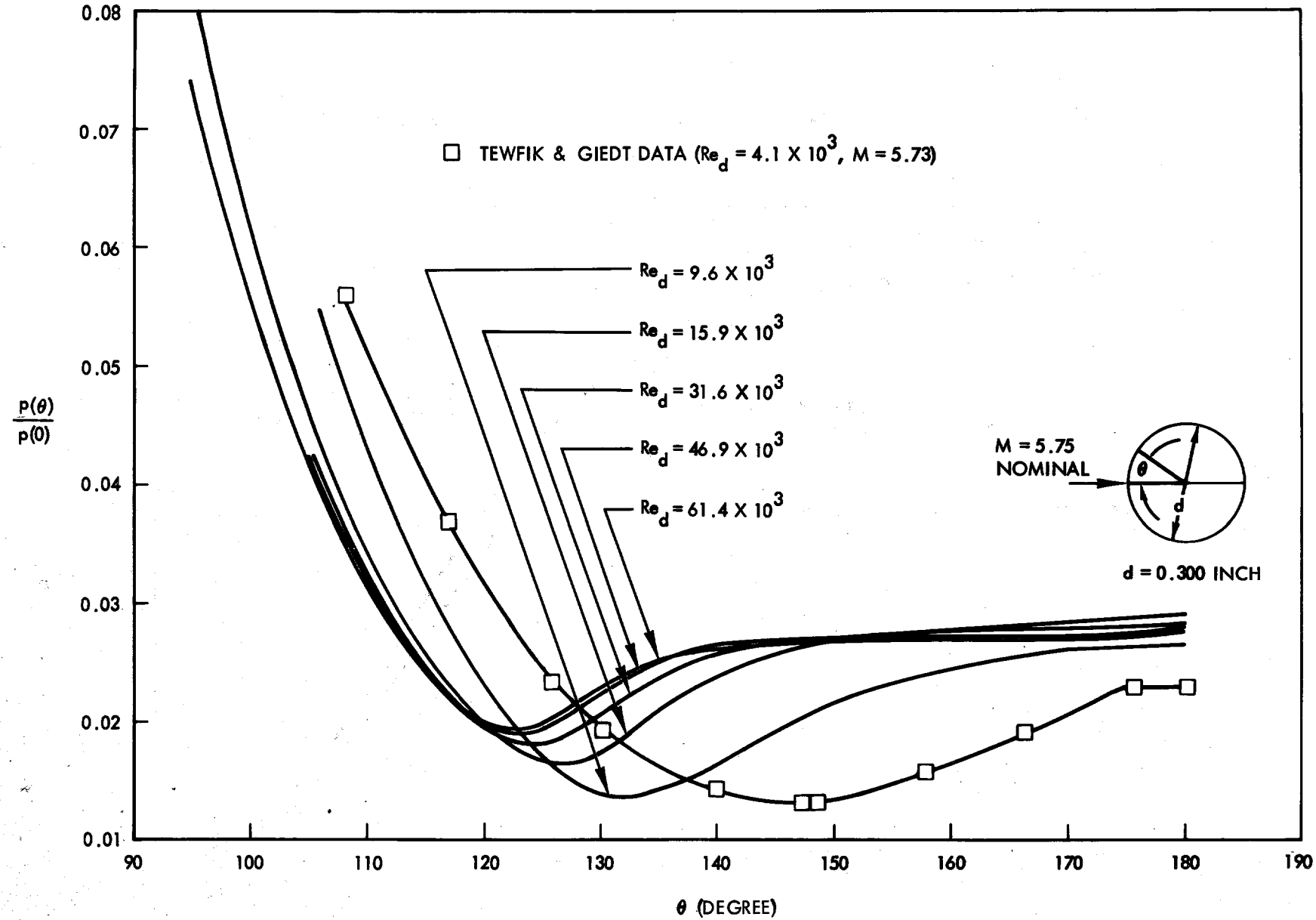

(b) Base Pressure

Figure 18. Experimental Pressure Distribution on Cylinder

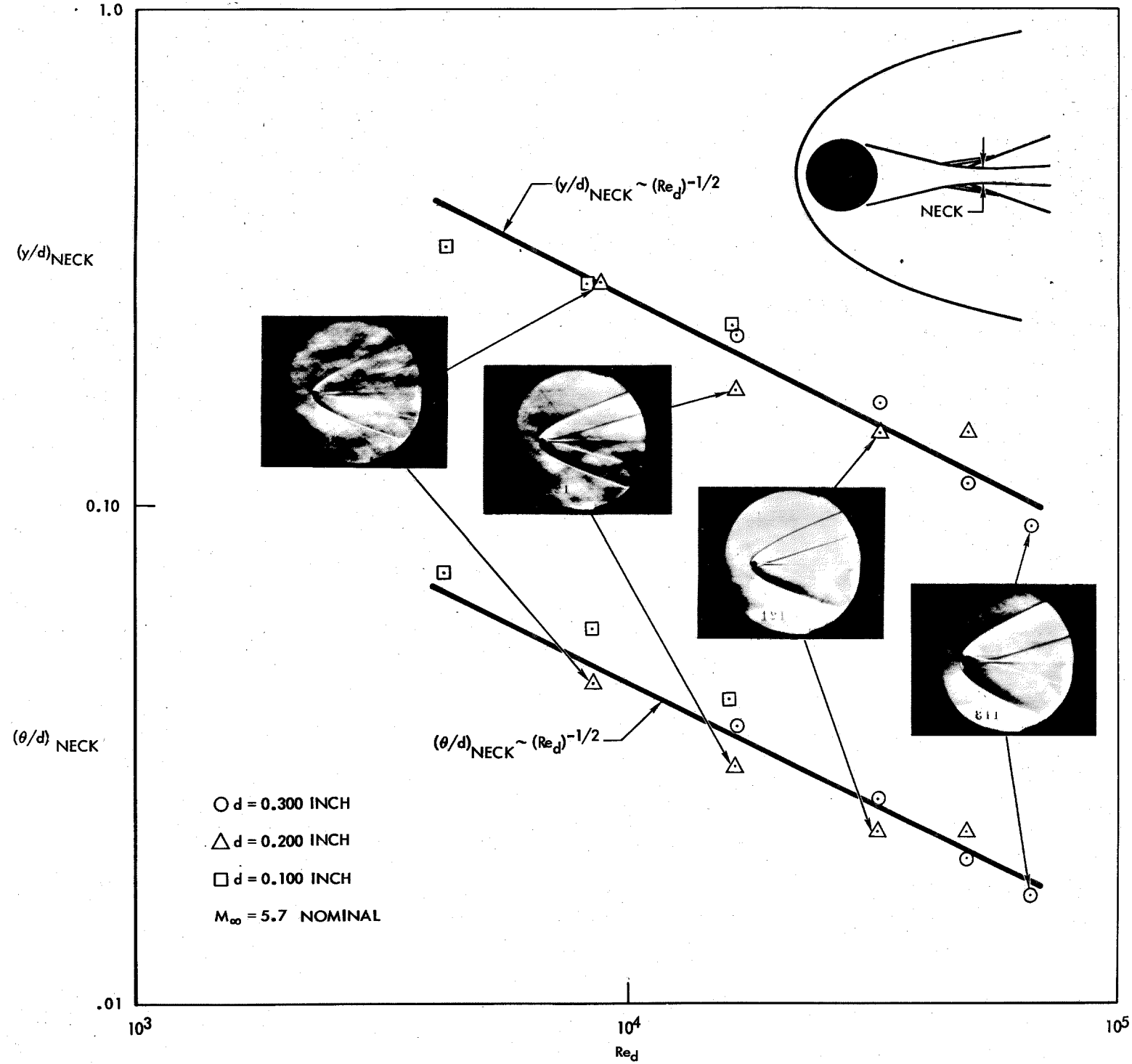

Figure 19. Wake Width and Momentum Thickness at Neck

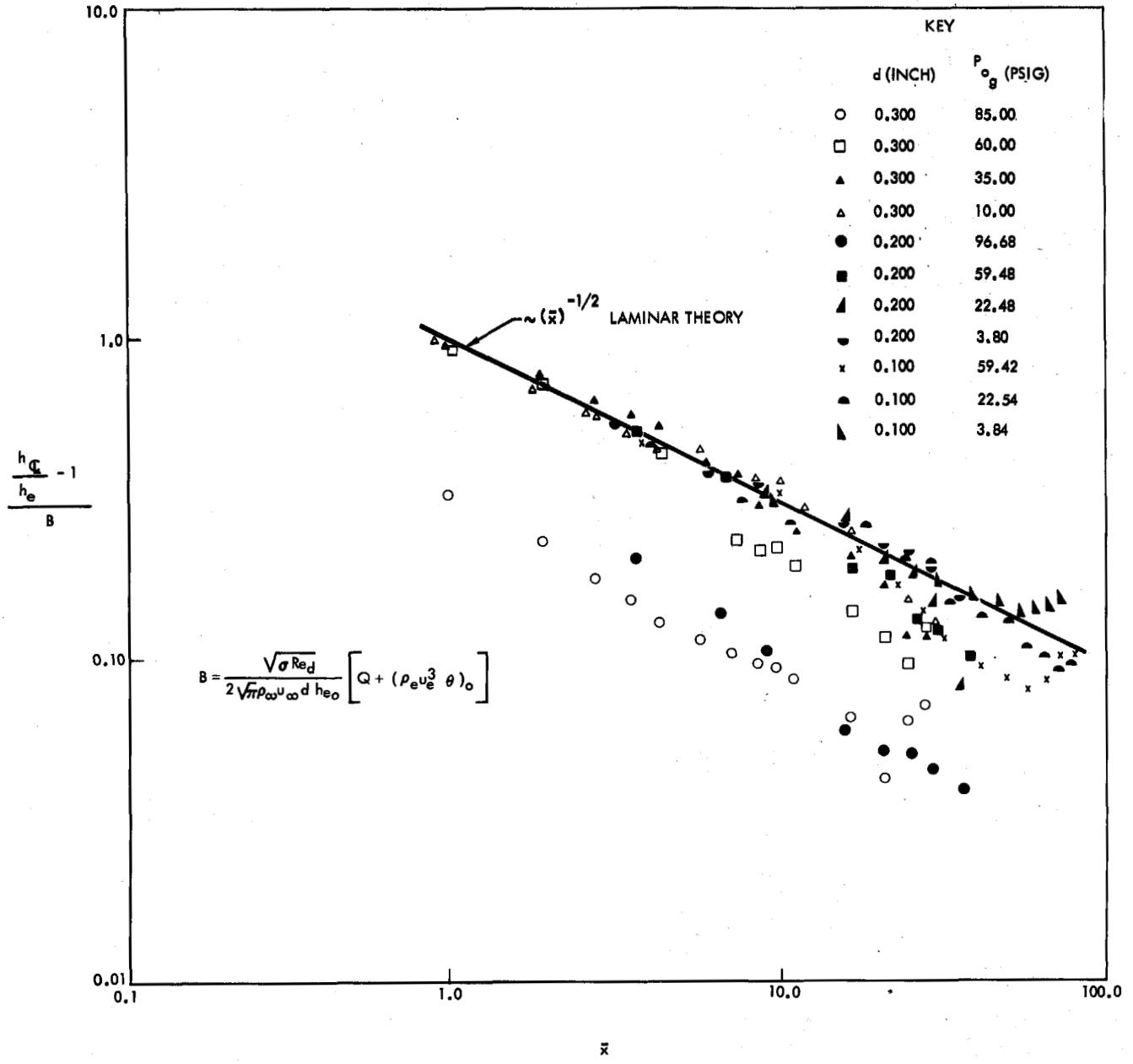

Figure 20. Static-Enthalpy Excess Along Wake Centerline

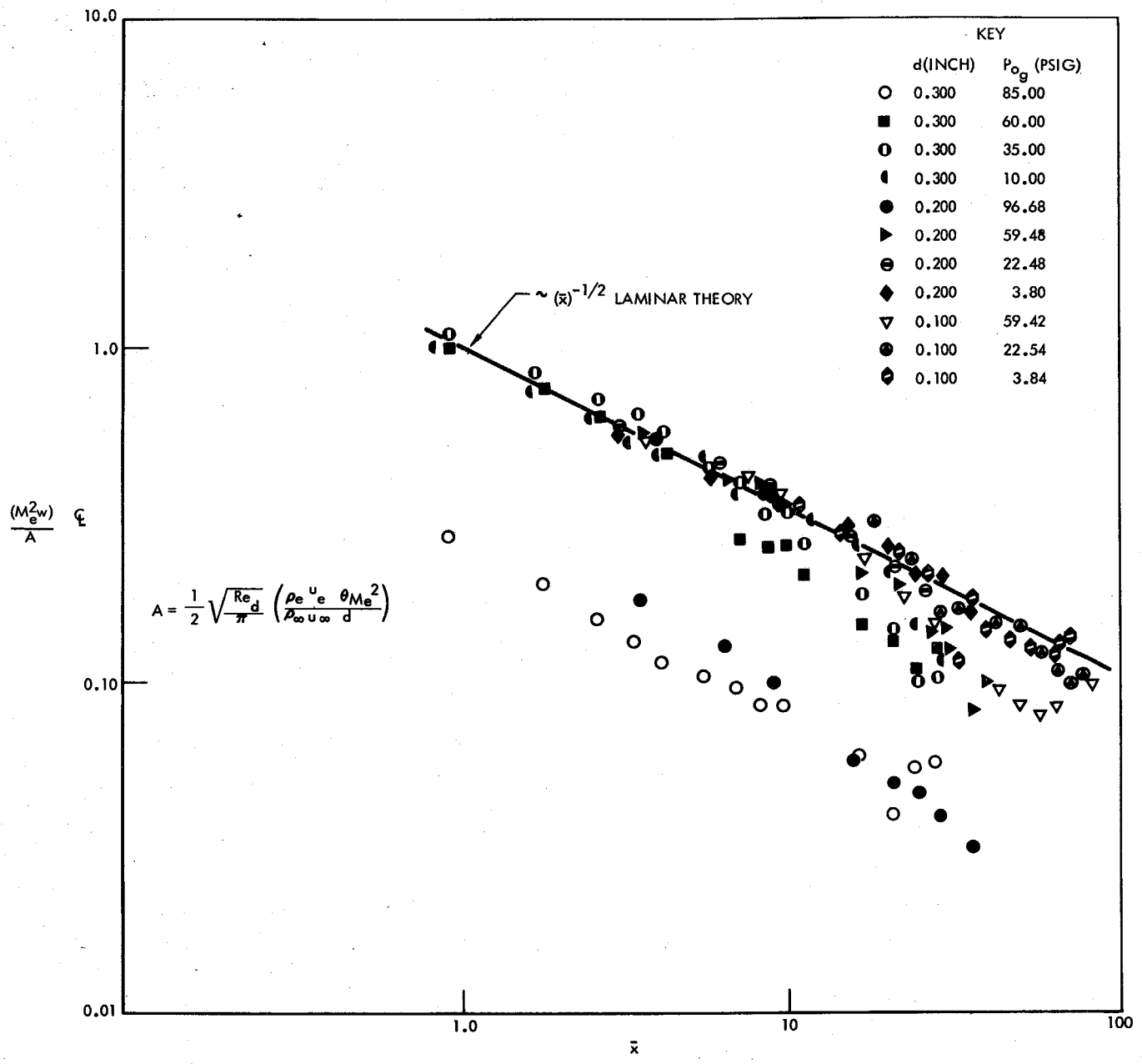

Figure 21. Velocity Defect Along Wake Centerline

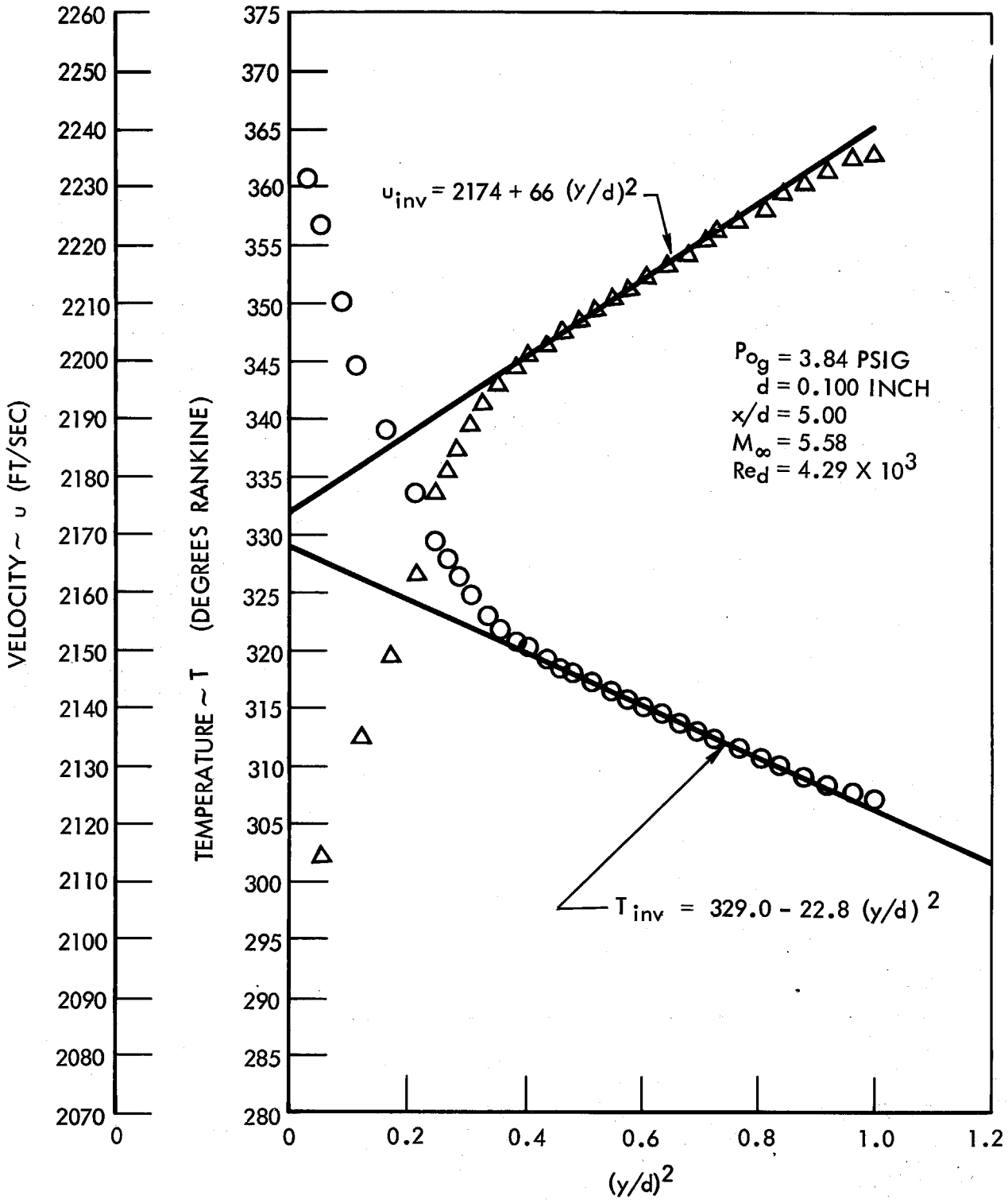

Figure 22. Determination of Inviscid Values of Velocity and Temperature

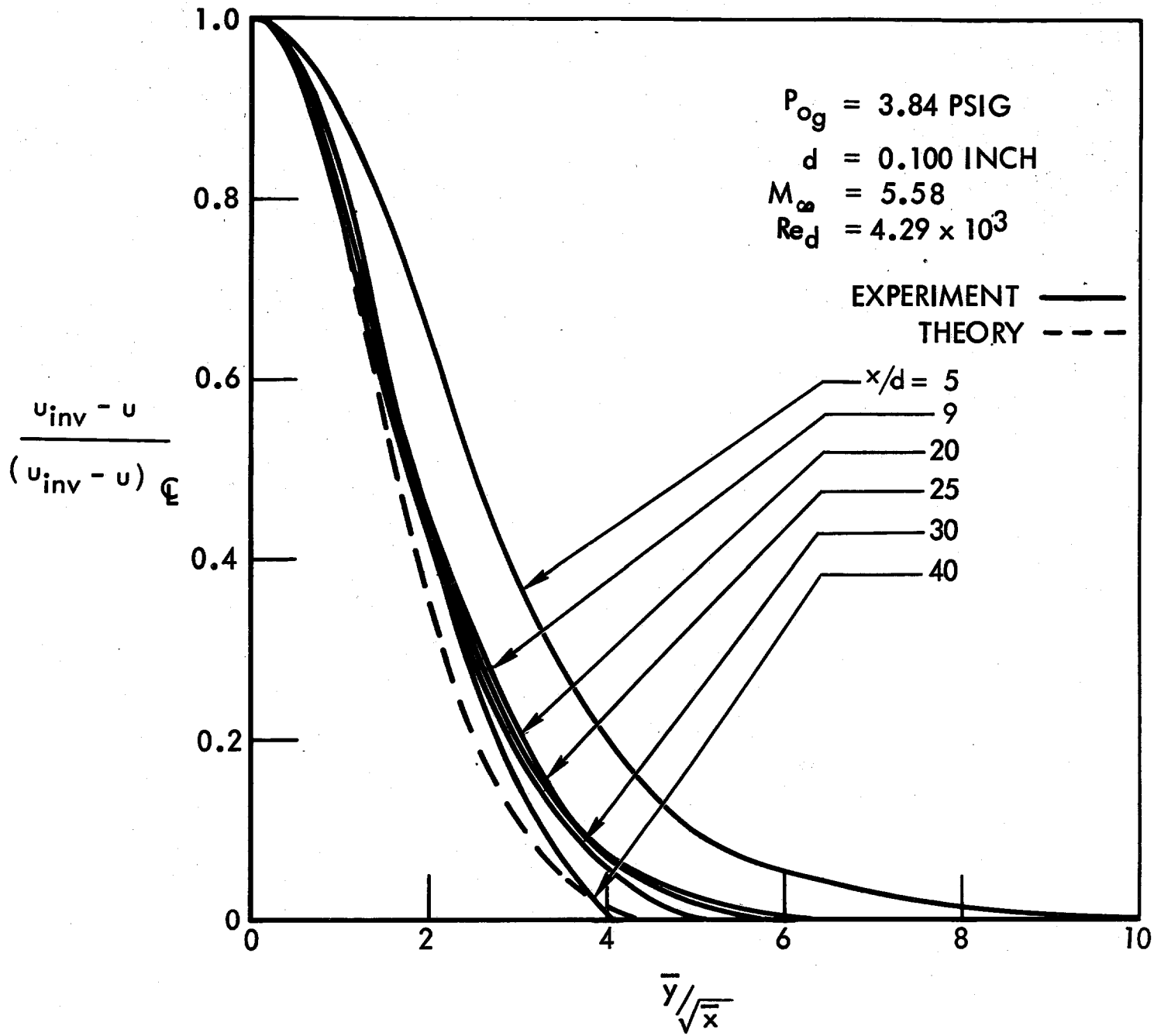

(a) Velocity

Figure 23. Normalized Profiles, 0.100-Inch Diameter Cylinder

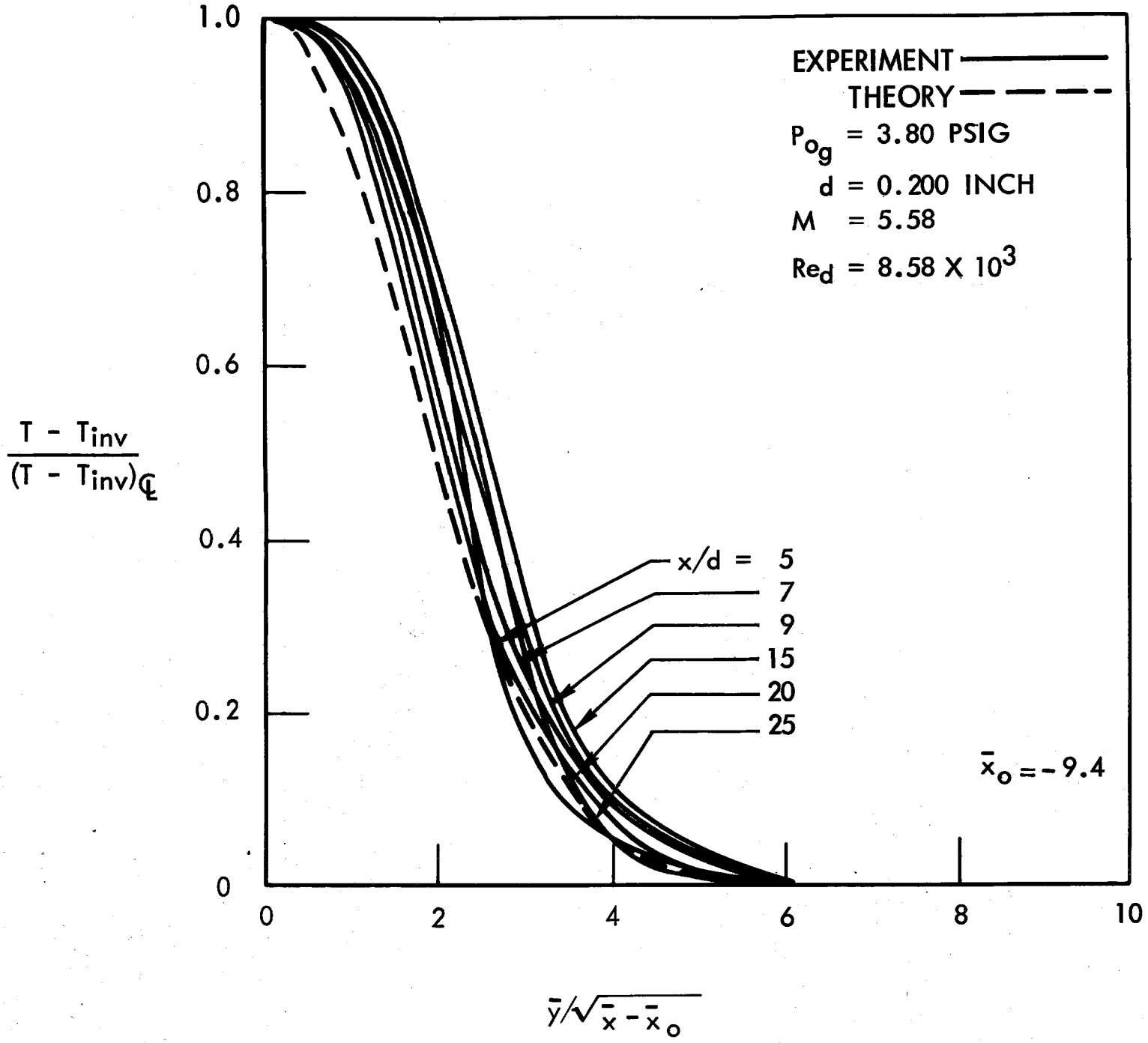

(b) Temperature

Figure 24. Normalized Profiles, 0.200-Inch Diameter Cylinder

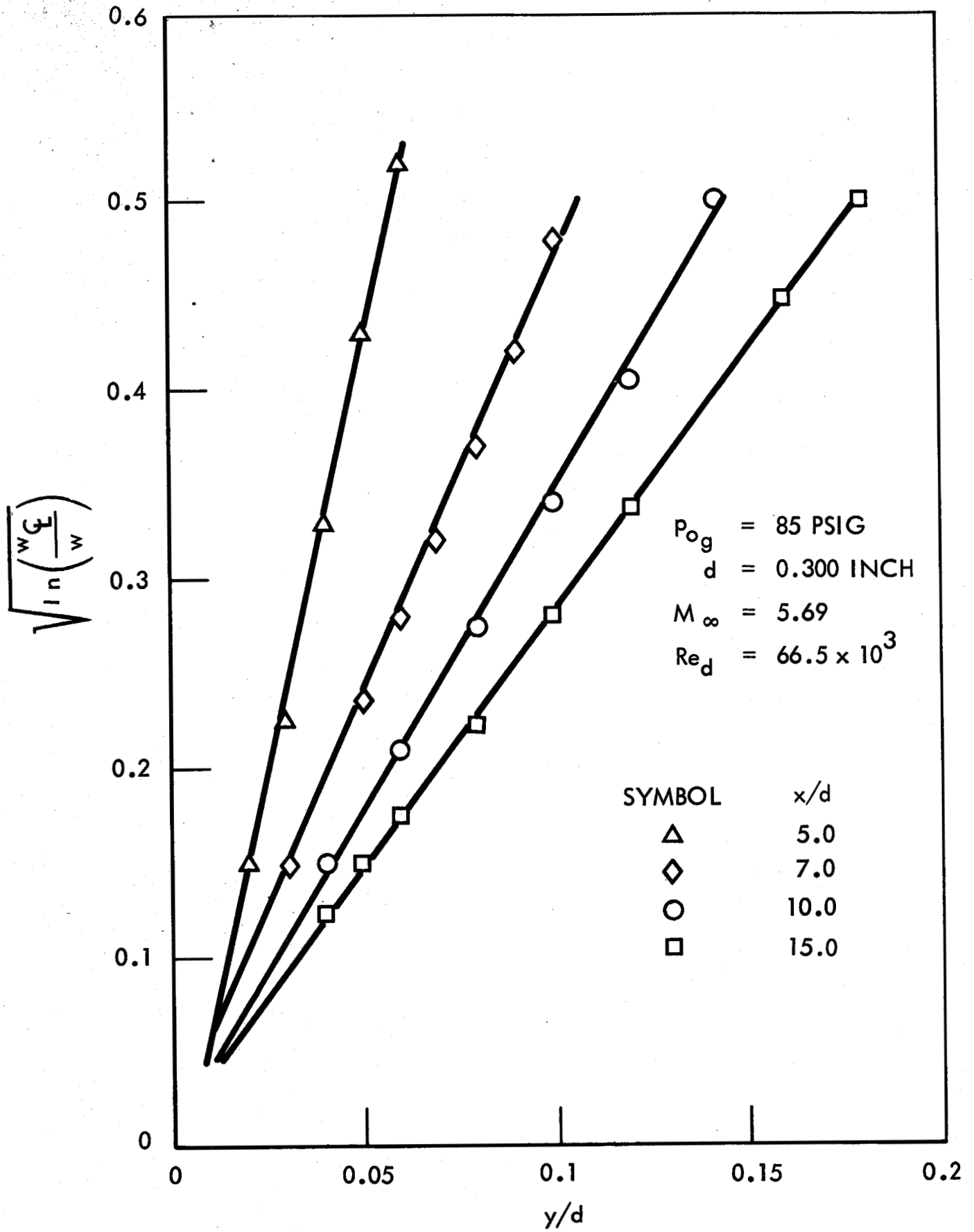

Figure 25. Determination of Diffusivity Number

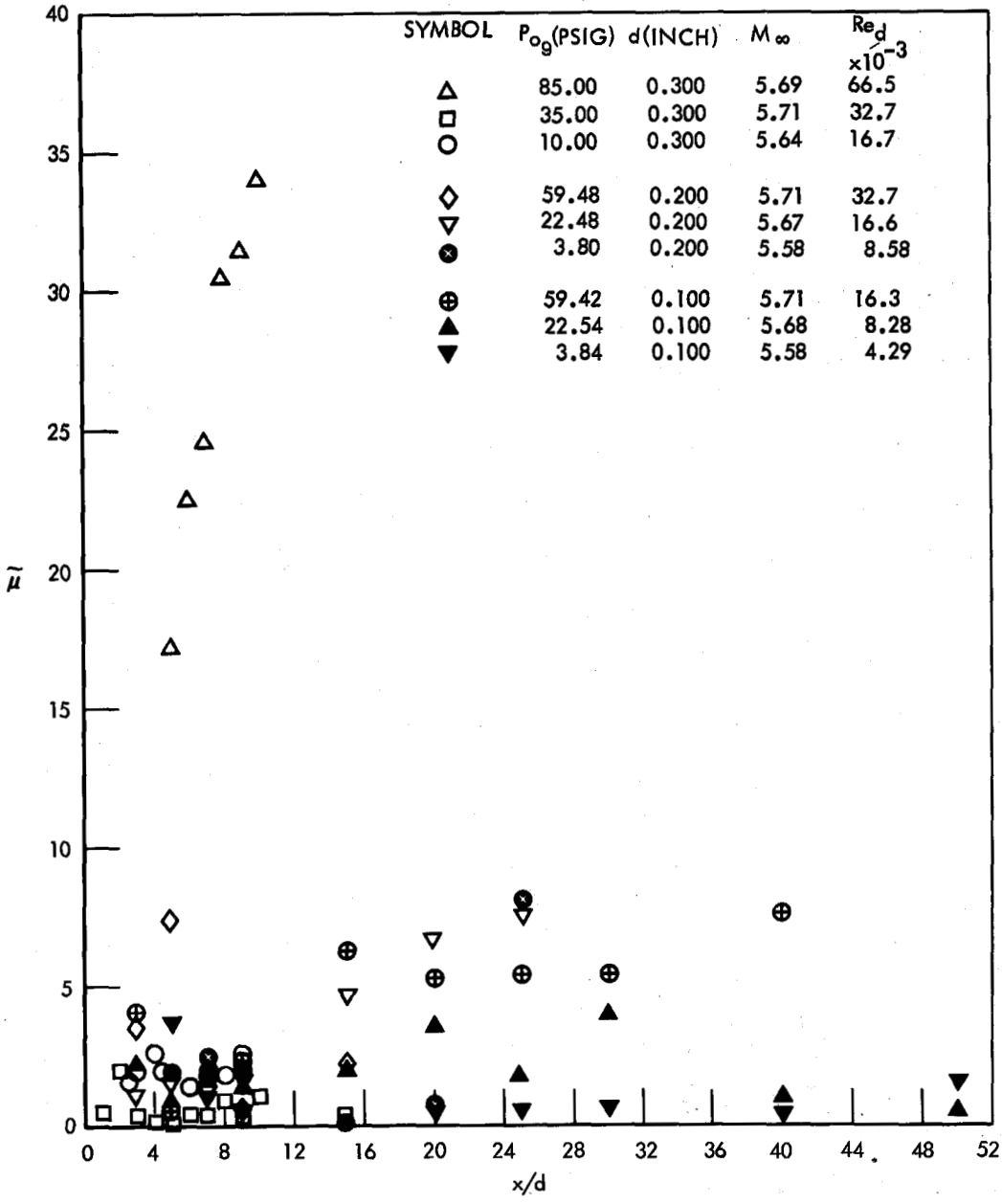

Figure 26. Viscosity Parameter Versus Axial Distance

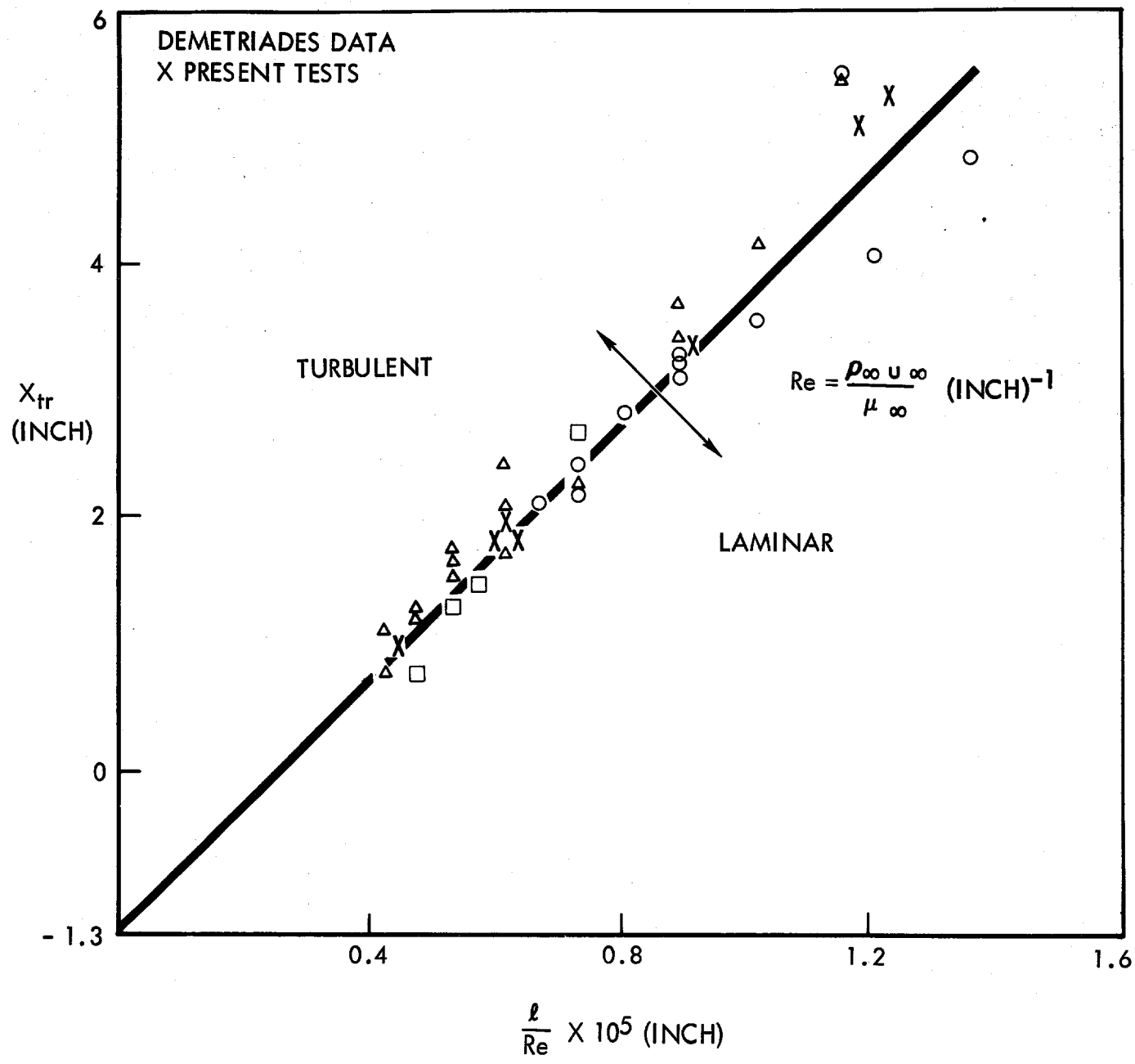

Figure 27. Transition